Enhancer-targeted CRISPR-Activation Rescues Haploinsufficient Autism Susceptibility Genes

George T. Chen[1,2], Gayatri Nair[1,2], Aubrey J. Osorio[1,2], Sandra M. Holley[3], Kimiya Ghassemzadeh[1,2], Jose Gonzalez[1,2], Congyi Lu[6-7], Neville E. Sanjana[6-7], Carlos Cepeda[3], Daniel H Geschwind[1-5]

1 Program in Neurogenetics, Department of Neurology, David Geffen School of Medicine, UCLA, Los Angeles, CA

2 Center for Autism Research and Treatment, Semel Institute, UCLA, Los Angeles, CA

3 Intellectual and Developmental Disabilities Research Center (IDDRC), Department of Psychiatry and Behavioral Sciences; David Geffen School of Medicine, UCLA, Los Angeles, CA

4 Department of Human Genetics, David Geffen School of Medicine, UCLA, Los Angeles, CA

5 Institute of Precision Health, David Geffen School of Medicine, UCLA, Los Angeles, CA

6 New York Genome Center, New York, NY

7 Department of Biology, New York University, New York, NY

Corresponding Author: dhg@mednet.ucla.edu

Abstract

Autism Spectrum Disorder (ASD) is a highly heritable condition with diverse clinical presentations. Approximately 20% of ASD's genetic susceptibility is imparted by *de novo* mutations of major effect, most of which cause haploinsufficiency. We mapped enhancers of two high confidence autism genes – *CHD8* and *SCN2A* and used CRISPR-based gene activation (CRISPR-A) in hPSC-derived excitatory neurons and cerebral forebrain organoids to correct the effects of haploinsufficiency, taking advantage of the presence of a wildtype allele of each gene and endogenous gene regulation. We found that CRISPR-A induced a sustained increase in *CHD8* and *SCN2A* expression in treated neurons and organoids, with rescue of gene expression levels and mutation-associated phenotypes, including gene expression and physiology. These data support gene activation via targeting enhancers of haploinsufficient genes, as a therapeutic intervention in ASD and other neurodevelopmental disorders.

Introduction

Autism Spectrum Disorders (ASD) are neurodevelopmental disorders characterized by impaired social behaviors and repetitive behaviors, often with severe functional impairment. ASD is highly prevalent, affecting approximately 1 in 54 individuals across all racial, ethnic, and socioeconomic groups, and thus presents a significant public health burden (Maenner et al., 2020). Although it is highly heritable, a substantial fraction of genetic susceptibility, perhaps up to 20% (Gaugler et al., 2014), is imparted by *de novo* mutations with major effects (15-20%)(Geschwind & State, 2015; Vorstman & Scherer, 2023).

Studies in large cohorts of patients and their families – such as the Simons Simplex Collection (SSC), and the Autism Genetic Resource Exchange (AGRE) have identified hundreds of genes increasing autism risk with various levels of statistical support, most via harboring *de novo* mutations (Cirnigliaro et al., 2023; Fu et al., 2022; Iossifov et al., 2014; Ronemus et al., 2014; Ruzzo et al., 2019; Sanders et al., 2012; Satterstrom et al., 2020). These "high-confidence" ASD genes (hcASD) are particularly enriched in genes that regulate gene expression or synaptic development during the peak of cortical neurogenesis (Parikshak et al., 2013; Satterstrom et al., 2020; Schafer et al., 2019). Studies in model systems also strongly implicate haploinsufficiency as the underlying mechanism of mutation (Collins et al., 2020; Gompers et al., 2017; T. N. Huang et al., 2014; Platt et al., 2017; Tatsukawa et al., 2019). This model is further supported by the observation that virtually all susceptibility genes are strongly depleted for heterozygous protein truncating variants in humans (Fu et al., 2022; Lek et al., 2016; Morrill & Amon, 2019; Veitia & Potier, 2015), which indicates that hcASD genes are highly dosage sensitive and require both alleles for normal function.

Here, we focused on two well-characterized hcASD risk genes, Chromodomain Helicase DNA-binding protein 8 (*CHD8*) and Sodium channel protein type 2 subunit alpha (*SCN2A*) (de la Torre-Ubieta et al., 2016; Rolland et al., 2023). *CHD8* is one of the most strongly associated genes with ASD, and it appears to regulate many other hcASD risk genes involved in neurodevelopment and synaptic function (Bernier et al., 2014; Durak et al., 2016; Platt et al., 2017; Villa et al., 2020; Weissberg & Elliott, 2021).The *SCN2A* gene encodes the voltage-gated sodium channel $Na_V1.2$ which is essential for the generation and propagation of action potentials in neurons, and is

mutated in Dravet Syndrome and other sodium channelopathies (Ben-Shalom et al., 2017; Wolff et al., 2017). The distinct roles of these two genes are evident in their normal patterns of expression in cortical development; *CHD8* peaks during neurogenesis and decreases over time, while *SCN2A* is expressed later, but still during mid- fetal development. Thus, in studying these two genes, we aimed to interrogate the efficacy of applying CRISPR-A during development.

Since haploinsufficient genes are also highly dosage sensitive (Collins et al., 2022), we hypothesized that enhancer-targeting would allow for more nuanced control of gene expression and avoid cell toxicity effects from gene overexpression, which is more likely from promoter regions (Morrill & Amon, 2019; Savell et al., 2018). To upregulate gene expression, we identified potential enhancers for CHD8 and SCN2A predicted to be active during fetal brain development by leveraging our previous work identifying gene expression regulatory elements in human brain *in vivo* and *in vitro* (de la Torre-Ubieta et al., 2018; Won et al., 2016, 2019). We demonstrate that targeting these enhancer sequences significantly increased target gene expression, while maintaining the trajectory of expression across development in a cerebral organoid model system and in differentiating excitatory neurons. Core phenotypes, including over-proliferation in *CHD8*$^{+/-}$ and electrophysiological abnormalities in *SCN2A*$^{+/-}$ are also rescued by CRISPR-A for several months post-treatment. Taken together, our results indicate that enhancer-targeted CRISPR-A can rescue gene expression levels and mutant phenotypes, supporting the potential for using enhancer-targeted gene activation as a therapeutic approach in ASD.

Results

CHD8 haploinsufficiency leads to increased organoid size and over-proliferation of progenitor cell populations

Stem cell lines edited to be haploinsufficient for *CHD8* (Shi et al., 2023) or *SCN2A* (Lu et al., 2019) were first characterized by establishing 2-dimensional excitatory neuron cultures and 3-dimensional cerebral forebrain organoids (hCO; (Pașca et al., 2022)) from each line to identify aberrant phenotypes to target for rescue (Figure 1A; Methods).

For each of the two *CHD8*-mutant lines, we first confirmed the presence of the edit in the genomic DNA (Supplemental Figure 1). We expect that the mutation of a single allele would lead to an approximately 50% reduction in mRNA and protein levels compared to the parental wildtype (HUES66), which we observed in both *CHD8*-mutated lines (CHD8-1, CHD8-2; Figure 1B, 1C). We next established cortical organoids from all three lines, using a protocol that previously shown to accurately recapitulate many features of *in vivo* cortical development (Gordon et al., 2021; Pasca et al., 2015). *CHD8* mRNA expression was consistently decreased in mutant hCO from day 50 to 200 compared to the parental line (Figure 1D) and was also reflected in a decrease in protein level as measured by immunofluorescence (Figure 1E&F). The expression trajectory of *CHD8* reflects *in vivo* patterns observed in human cortical development, peaking in the first and early second trimesters and decreasing gradually past late childhood (Supplemental Figure 2).

One of the most well-characterized phenotypes resulting from *CHD8* haploinsufficiency in affected individuals is macrocephaly (Bernier et al., 2014). We therefore measured hCO sizes at multiple timepoints and found that at both 50- and 70-days post-initiation, hCO produced from *CHD8* mutant lines were significantly larger than wildtype (Figure 1G). To determine if this size difference was the result of increased proliferation or increased cell size, we first measured the

size of cell nuclei and found a significant increase in nuclear size in both CHD8 mutant lines (Figure 1H). To measure changes in proliferation, we performed flow cytometry on dissociated hCO (Methods). We observed an increase in the proportion of cells in the S/G2/M phases (Figure 1I) in mutant organoids. Additionally, we labeled the dissociated cells with antibodies for Sox2, Tbr2, and NeuN, as markers for neural stem cells, neural progenitors, and neurons, respectively. By flow cytometry, we looked specifically at the cells in the S/G2/M phases as identified by EdU and found a larger proportion of Tbr2+ cells in mutant hCO (Figure 1J), suggesting that an over-proliferation of neural progenitor cells is responsible for the macrocephaly phenotype. We confirmed this by immunofluorescence, observing a broadening of the $Tbr2^{+}$ cell layer in CHD8-mutant hCO, indicating an expansion of the neural progenitor population (Figure 1K). This agrees with recent published work (Paulsen et al., 2020) using the same $CHD8^{+/-}$ lines, but a different protocol to create cortical organoids for characterization by single cell RNA sequencing (Supplemental figure 3). Specifically, scRNAseq of three-month old organoids showed a decrease in excitatory neurons in $CHD8^{+/-}$ organoids compared to wildtype and an increase in multiple progenitor cell populations, including cells from glial lineages. We observe this in our hCO cultures by qPCR and immunofluorescence for markers of glial progenitors (Supplemental figure 4). Collectively, these results demonstrate that the hCO system recapitulates the patient macrocephaly phenotype, and that this enlargement is caused by an over-proliferation of progenitor cells early in development.

SCN2A haploinsufficiency leads to aberrant excitatory neuron phenotypes

The *SCN2A* mutation was first confirmed in the mutant stem cell line by Sanger sequencing (Supplemental Figure 1). We validated the effect of this mutation in expression levels of *SCN2A* mRNA and protein (Figure 2A, 2B). Unlike the $CHD8^{+/-}$ lines, in the hCO from $SCN2A^{+/-}$ cells, we observed that *SCN2A* expression did not significantly diverge in expression levels compared to the wildtype hCO until after 120 days of culture (Figure 2C). This observation is consistent with the expression of *SCN2A* in human cortical development, where *SCN2A* increases monotonically during fetal cortical development, reaching an asymptote around birth (Supplemental Figure 2;(Brunklaus & Lal, 2020)). Using immunofluorescence, we analyzed Scn2a protein expression levels at 90-, 150-, and 180-days post-initiation. The percentage of Scn2a-positive cells was significantly decreased in mutant organoids at each measured timepoint (Figure 2D, 2E).

We next analyzed the expression of *EOMES* and *SATB1* as markers of intermediate progenitor cells and upper layer neurons, respectively, cells that are well-represented at this time. Mirroring the trajectory of *SCN2A* expression, both *EOMES* and *SATB1* show significant decreases in expression only at later timepoints (Figure 2F). We additionally established excitatory neuron cultures using *NGN2* overexpression (Zhang et al., 2013) and performed whole-cell patch-clamp electrophysiology on individual neurons (Figure 2G). Cells formed synaptic connections and exhibited spontaneous postsynaptic current (PSC) events of varying frequencies, possibly influenced by the extent of cellular confluence (HUES66: mean = 2.83±0.83 Hz, range = 0.23-9.85 Hz; $SCN2A^{+/-}$: mean = 2.05±0.86 Hz, range = 0.04-9.67 Hz). Compared to the wildtype line, $SCN2A^{+/-}$ mutant neurons generated a much weaker response to a sustained, depolarizing current injection (Figure 2H, and Figure 6D, 6E). We also observed a trend for smaller sodium currents in the mutant neurons (Figure 2I, 2J), as well as a trend for increased input resistance (Figure 2K), consistent with reduced physiological maturity. Taken together, these results show that *SCN2A* haploinsufficiency results in impaired development and function of excitatory neurons.

147

148 ## Enhancer-targeted guideRNA increase expression of CHD8 and SCN2A using CRISPR-A

149 We hypothesized that using CRISPR-A to drive increased expression of the non-mutant
150 allele of haploinsufficient genes would be an effective approach towards rescuing mutant
151 phenotypes. One key issue in using CRISPR-A to compensate for haploinsufficiency is the potential
152 deleterious effects on cell fitness caused by overexpression, which is a frequent consequence of
153 targeting gene promoters (Matharu et al., 2018). This is especially a concern with
154 haploinsufficient genes, which are notoriously dosage sensitive (Fu et al., 2022; N. Huang et al.,
155 2010). We therefore chose to target gene enhancers rather than promoters, with the rationale
156 that endogenous gene expression regulation would be matched more closely across
157 developmental time and cell type specific expression would be preserved (de la Torre-Ubieta et
158 al., 2018; Won et al., 2019). To date, no published studies targeting hcASD genes have used
159 enhancer-targeted CRISPR-A, as few putative enhancers have been validated. We first identified
160 enhancer regions to target (Methods) by combining previously published maps of fetal human
161 brain genome using ATAC-seq (de la Torre-Ubieta et al., 2018) and Hi-C (Won et al., 2016) with a
162 broader list of adult human brain enhancers generated by the PsychENCODE Consortium (D.
163 Wang et al., 2018). We focused primarily on fetal brain enhancers, as they were more likely to be
164 relevant during the time points that we examined. Using these maps (Table 1, Supplemental
165 Figure 5), we identified four putative human fetal brain enhancers for *CHD8* and three for *SCN2A*.
166 After filtering (Methods), we synthesized three guide RNA per enhancer, for a total of six *CHD8*
167 gRNA candidates and three *SCN2A* gRNA candidates (Figure 3A).

168 For *CHD8*, the two targeted enhancers flanked opposing ends of the gene (Figure 3B, full
169 map in Supplemental Figure 5). We first screened the candidate gRNA in HEK293T cells, co-
170 transfecting the guideRNA with a dCas9-p300 plasmid. We chose to use dCas9-p300 because it is
171 an endogenous regulator of gene expression, as opposed to other synthetic activation constructs
172 (Hilton et al., 2015). Of the six guides tested, only two, CHD8-g1 and CHD8-g5, significantly
173 increased *CHD8* expression, one for each of the enhancers (Figure 3C). As an additional validation
174 step, we transduced the guides into primary human neural progenitor cells (phNPCs) to
175 determine if the identified enhancers were active in a more physiologically relevant model system
176 (Figure 3D). Both guides significantly increased *CHD8* expression in phNPCs. Finally, we screened
177 the guides in hCO, using a stem cell line constitutively expressing dCas9-p300. We established
178 dCas9-p300 hCO and cultured them for fifty days prior to infection with the guide RNA. Both
179 guides increased *CHD8* expression over control (Figure 3E), indicating that a single treatment was
180 durable across several months of development.

181 After filtering (Methods), only one human fetal brain enhancer was targeted for *SCN2A*
182 activation (Figure 3F, full map in Supplemental Figure 5). Of the three guides screened in HEK293
183 cells, one, SCN2A-g3, produced a significant increase in SCN2A expression level (Figure 3G), which
184 also significantly increased expression in phNPCs (Figure 3H). As a parallel set of experiments, we
185 also identified non-fetal brain enhancers for *SCN2A* from the PsychENCODE dataset and screened
186 additional guide RNAs, finding one additional enhancer gRNA that increased expression
187 (Supplemental Figure 6). Additionally, we tested dCas9-VPR as an alternate CRISPR-A vector but
188 found no significant improvement in gene activation (Supplemental Figure 5). In dCas9-p300
189 organoids, we transduced the gRNA after fifty days in culture and collected organoids for 3

months post-infection. We observed an increase in *SCN2A* expression across all measured timepoints, validating the durability of the CRISPR-A treatment (Figure 3I).

CRISPR-A treatment increases *CHD8* and *SCN2A* expression in haploinsufficient organoids and neurons

We next applied the CRISPR-A system to the haploinsufficient hCO models. For each gene, we first established mutant lines constitutively expressing the validated guide RNA by flow cytometry prior to creating hCO (Methods). We then applied CRISPR-A at the stages of developmental timepoints overlapping with robust expression of *CHD8* or SCN2A (Figure 1D, 2C). Additionally, as a complementary approach, we established 2D excitatory neuron cultures derived by *NGN2* overexpression (Lu et al., 2019; Zhang et al., 2013) and treated the neurons with CRISPR-A.

For *CHD8*, we infected mutant and wildtype cortical organoids at 25 days post-initiation (Figure 4A) and collected samples monthly for three months for RNA. In the wildtype hCO, we observed no increase in *CHD8* expression, consistent with observations from other groups using CRISPR-A on haploinsufficient genes (Colasante et al., 2019). In both *CHD8*-mutant lines, *CHD8*-g5 induced increases in CHD8 expression. Consistent with CHD-8's early peak expression *in vivo* and *in vitro*, the effect was lost after two months in CHD8-2 and three months in CHD8-1 (Figure 4B). CHD8-g1 only led to a moderate increase in *CHD8* expression in CHD8-1 hCO, although this result is consistent with our previous screen in dCas9-p300 wildtype hCO, which showed CHD8-g1 inducing a lower increase in *CHD8* expression than CHD8-g5 (Figure 3E). However, in excitatory neuron cultures, both guides generated robust increases in *CHD8* expression in both *CHD8*$^{+/-}$ lines during differentiation, with the most significant increases at 28-35 days post-induction (Figure 4C). We found that this difference in effect of CRISPR-A was largely due to a difference in dCas9-p300 expression (Supplemental Figure 7). Nonetheless, these results indicate that *CHD8* expression can be effectively increased by enhancer-targeted CRISPR-A.

As *SCN2A* expression peaks later in development, we infected wildtype and mutant cortical organoids at 120 days post-initiation (Figure 4D) and collected samples monthly for up to five months post-infection. We observed no significant increase in *SCN2A* expression in wildtype hCO, matching the observation of the same organoids treated with *CHD8* gRNA. However, we found a significant increase in *SCN2A* expression in *SCN2A*$^{+/-}$ hCO across all timepoints measured, though the degree of increase decreased over time (Figure 4E). We also established excitatory neuron cultures from the *SCN2A*$^{+/-}$ line using *NGN2* overexpression and observed the same result; no change in *SCN2A* levels in wildtype neurons, but a significant increase in *SCN2A* mRNA and protein levels in the mutant line treated with CRISPR-A. These results demonstrate that *SCN2A* expression can be reliably increased by enhancer-targeted CRISPR-A.

CRISPR-A treatment rescues mutant phenotypes in CHD8 and SCN2A cortical organoids and neurons

To further study the over-proliferation of progenitor cells caused by CHD8 haploinsufficiency, we quantified the expression of Tbr2 and Dcx proteins in two-dimensional (2-D) excitatory neuron cultures (Figure 5A). Compared to wildtype neurons, the CHD8-mutant neurons had significantly higher numbers of Tbr2+ cells and significantly lower numbers of Dcx+

233 cells, suggesting a larger population of intermediate progenitor cells. Mutant neurons infected
234 with dCas9-p300 showed a significant decrease in Tbr2 expression and significant increase in Dcx
235 expression to levels near wildtype across both guide RNAs and both mutant lines (Figure 5B).
236 Additionally, significantly more Dcx+ cells were found to be present along cell processes (Figure
237 5C). We quantified mRNA expression of *EOMES*, *DCX*, *TUBB3*, and *MAP2*, as markers for
238 intermediate progenitors, immature neurons, and mature neurons, respectively, and observed a
239 decrease in *EOMES* expression and increase in neural marker expression in treated excitatory
240 neuron cultures (Figure 5D). Collectively, these results suggest that the overabundant progenitor
241 phenotype caused by CHD8 haploinsufficiency is rescued by our enhancer-targeted CRISPR-A.
242 As we observed in our initial characterization, *CHD8*$^{+/-}$ hCO are significantly larger than
243 wildtype at matched timepoints, a phenotype caused by an increase in progenitor cell
244 proliferation, as previously observed (Paulsen et al., 2022; Villa et al., 2020). We measured hCO
245 size monthly after infection with dCas9-p300. For CHD8-1, both guides lead to decreased organoid
246 size compared to the vehicle-treated control, significant after 1 month with CHD8-g1 and after
247 three months with CHD8-g5. CHD8-2 hCO decreased with CHD8-g1 infection but exhibited a small
248 but significant decrease after one month with CHD8-g5 (Figure 5E). By comparison, no significant
249 size changes were observed in wildtype HUES66 hCO treated with either CHD8-targeting guide.
250 We next performed RNAseq in CHD8 mutant and wildtype day 50 hCO, identifying 5,933
251 significant genes differentially expressed (Methods; Figure 5F); 2,608 upregulated and 3,325
252 down-regulated in CHD8$^{+/-}$ hCO. Treatment of the CHD8$^{+/-}$ hCO with CRISPR-A reverted gene
253 expression levels towards wildtype, substantially reducing the number of differentially expressed
254 genes relative to the wildtype (3,172 genes differentially expressed; 1,811 upregulated and 1,361
255 downregulated) and untreated mutant hCO (1,039 genes differentially expressed; 802
256 upregulated and 237 downregulated). Unbiased clustering grouped the CRISPR-A-treated
257 samples in between wildtype and untreated mutant samples, indicating that CRISPR-A infection
258 lead to a shift in expression towards wildtype (Figure 5G). Gene Ontology (GO) analysis of
259 significantly upregulated genes in both HUES66 and CHD8$^{+/-}$ + CRISPR-A hCO showed significant
260 enrichment for GO terms associated with neuron maturation; including neuron projection, axon
261 guidance, and cortical actin cytoskeleton, further evidence that our enhancer-targeted CRISPR-A
262 rescues CHD8$^{+/-}$ mutant phenotypes associated with neurogenesis and maturation (Figure 5H).
263 To determine the efficacy of using CRISPR-A to increase *SCN2A* expression, we focused on
264 phenotypes related to neuron maturation and function, as these would be most directly impacted
265 by *SCN2A* mutation. We previously observed both *EOMES* and *SATB2* to be significantly decreased
266 in mutant hCO compared to wildtype at late stages of development (Figure 2F). Infecting *SCN2A*$^{+/-}$
267 hCO with CRISPR-A lead to an increase in both *EOMES* and *SATB2* expression that was sustained
268 over the timepoints measured, though sample-to-sample variation between infected organoids
269 was high, suggesting an inconsistent level of phenotype rescue. We therefore measured
270 expression of cell type markers in 2D differentiated excitatory neuron cultures and found a more
271 consistent, significant increase in both *EOMES* and *SATB2* mRNA levels in neurons infected with
272 CRISPR-A (Figure 6B). Additionally, we observed an increase Tuj1 and Map2 protein levels in
273 neurons infected with CRISPR-A (Figure 6C), collectively indicative of a rescue of neuron
274 maturation.
275 We next performed whole-cell patch-clamp recording on *SCN2A*$^{+/-}$ neurons with or
276 without CRISPR-A to determine whether there was rescue of the major physiological phenotype

observed in *SCN2A* haploinsufficiency. We were able to restore excitability to wildtype levels in *SCN2A*$^{+/-}$ + CRISPR-A neurons (Figure 6D&E). The addition of CRISPR-A significantly increased the number of action potentials fired in response to increasing current injections, reaching levels comparable to wildtype (Figure 6D, 6E). This occurred despite no notable differences in rheobase measurements and resting membrane potential (RMP), indicating a nearly complete restoration of neuron function and excitability (Supplemental Figure 8). Taken together, we demonstrate that the enhancer-targeted gRNA for *CHD8* and *SCN2A* rescued mutant phenotypes in hCO and induced neurons in 2D cultures.

Discussion

There are few currently available therapies other than symptomatic treatments for ASD, whose efficacy are limited by clinical and genetic heterogeneity. Here we leveraged the growth of nucleic acid therapeutics, which is a promising frontier, especially for the treatment of rare brain diseases (Chen & Geschwind, 2022; Ricci & Colasante, 2021; Sahin & Sur, 2015; Weuring et al., 2021; Whiteley et al., 2022). We hypothesized that by using CRISPR-A to target a haploinsufficient gene, one could increase the expression of the wildtype allele to restore gene expression to normal levels. CRISPR-A is more generalizable than other precision medicine technologies, as it may be more broadly applied to any individual with a haploinsufficient mutation in the given gene, as demonstrated in other disease models with some success. This includes *Sim1* in obesity (Matharu et al., 2018), *Scn1a* in Dravet Syndrome (Colasante et al., 2019), and others (Colasante et al., 2020; Tamura et al., 2022). It is worth noting that haploinsufficient genes have been shown in animal models to be embryonic lethal when knocked out, and their overexpression is associated with decreased fitness (Collins et al., 2020; N. Huang et al., 2010; Morrill & Amon, 2019), emphasizing the importance of moderating any induced increase in expression. With this in mind, we targeted enhancer regions, hypothesizing that endogenous mechanisms of gene expression regulation would better modulate the expression of *CHD8* and *SCN2A* when driven by enhancer activation. For both *CHD8* and *SCN2A*, we were able to significantly increase the expression of each gene in mutant hCO using a single enhancer-targeted gRNA paired with dCas9-p300. This increase in expression resulted in partial or complete rescue of mutant phenotypes; increase of *CHD8* lead to decreased organoid size, decreased progenitors, and increased neurons. Increase of *SCN2A* expression increased the expression of upper layer neuron markers and normalized excitability and neuronal firing in excitatory neuron cultures.

We replicate previous findings by showing the phenotype of over-proliferation in *CHD8* haploinsufficiency and electrophysiological abnormalities in *SCN2A* haploinsufficiency (Paulsen et al., 2022; Spratt et al., 2019), two monogenic causes of ASD that have very high penetrance for ASD (OR >100; (Rolland et al., 2023)). We observed a significant increase in size in *CHD8*$^{+/-}$ hCO compared to wildtype at matched timepoints, a phenotype that appears analogous to macrocephaly observed in patients (Bernier et al., 2014; Villa et al., 2020). The increase in size in *CHD8*$^{+/-}$ hCO resulted from an increase in progenitor cell proliferation, consistent with previously published studies using different brain organoid (Paulsen et al., 2022; Villa et al., 2020; P. Wang et al., 2017) and animal (Gompers et al., 2017) models. We also found *CHD8*$^{+/-}$ neurons to be less mature than wildtype, consistent with the role that *CHD8* and its downstream targets play in neurogenesis (Villa et al., 2020). In *CHD8*-deficient hCO and neurons, we were able to increase *CHD8* expression with CRISPR-A, resulting in a decrease in organoid size and increase in neuronal

differentiation. These results point to a rescue of neurogenesis, which has been highlighted in other studies (Gompers et al., 2017; Paulsen et al., 2022; P. Wang et al., 2017) as a key mutant phenotype.

The two *CHD8*$^{+/-}$ stem cell lines used in this study differ by only an additional four base pair deletion in CHD8-2 compared to CHD8-1 (Supplemental Figure 1, (Shi et al., 2023)). While the two lines both demonstrate decreased *CHD8* expression as stem cells, neurons, and organoids, we observed differences in organoid composition (Supplemental Figure 4), as well as response to CRISPR-A (Figures 4, 5). However, none of these differences reached statistical significance and differential gene expression analysis from bulk RNAseq data comparing CHD8-1 and CHD8-2 organoids yielded no significant DGE, so we are not sure what underlies the differences between these lines.

In *SCN2A*-deficient hCO, we observed a decrease in upper layer neurons compared to wildtype, specifically at later points in development, epochs at which *SCN2A* expression is expected to peak. These results are consistent with animal models that show impaired excitability in slices of prefrontal cortex (Eaton et al., 2021; Spratt et al., 2019; Yang et al., 2023). Neurons from this mutant line showed impaired excitability and reduced network activity, mirroring other studies that sought to model ASD-associated variants of *SCN2A* (Ben-Shalom et al., 2017; Tatsukawa et al., 2019). In *SCN2A*-deficient hCO and neurons, we were able to rescue gene expression to near wildtype levels and subsequently observe a rescue of signaling activity in excitatory neurons. Thus, we demonstrate the reversal of synaptic dysfunction, which was also recently demonstrated using a *SCN2A* promoter-targeting CRISPR-A system, where the investigators paid careful attention to avoid over-expression by using a less powerful activating construct (Tamura et al., 2022).

Despite our concerns of overexpression in using promoter-targeted gRNA constructs, work by other groups have targeted promoter regions of their genes of interest with no apparent impact on cell fitness (Colasante et al., 2019, 2020; Matharu et al., 2018; Tamura et al., 2022). We hypothesize that this may be due to endogenous regulatory mechanisms to limit gene overexpression in an organ-specific manner, or differing tolerances for gene overexpression based upon normal function. The former rationale was briefly explored in *Sim1* (Matharu et al., 2018), in which promoter and enhancer targeting guides were tested in multiple organ systems, with varying degrees of gene activation between organs. We note that in our *CHD8* experiments, we utilized two guide RNA constructs which exhibited differing levels of *CHD8* activation. As these guides targeted different enhancers, we hypothesize that differences between these enhancers accounts for differences in activation levels, which is a variable in need of further exploration in future studies.

We acknowledge that additional variables could be considered to further optimize gene expression rescue. First, the combined expression of both guide RNA and dCas9-p300 in organoids was limited by the ability of the dCas9-p300 lentivirus to infect only a subset of cells in the organoid (Supplemental Figure 7). We accounted for this by using NGN2 overexpression to establish excitatory neuron cultures from haploinsufficient lines to treat with CRISPR-A, which led to robust increases in *CHD8* and *SCN2A* expression and in dCas9-p300 mRNA levels. This indicates that further optimization of viral infection, constructs, and use of alternative Cas enzymes (Knott & Doudna, 2018) would be very useful.

363 Second, we noted the effect of CRISPR-A decreased over time, with a decrease in
364 expression of *CHD8* or *SCN2A* between two- and five-months post-infection. From the perspective
365 of paralleling endogenous expression during development this may be optimal, although it
366 suggests that rescuing adult expression may require targeting different enhancers or the gene
367 promoters. Third, there is evidence that multiple gRNA may exhibit synergistic effects when used
368 to target the same gene of interest (Hilton et al., 2015), though the same group noted that dCas9-
369 p300 appeared to have a moderately additive, rather than synergistic level of increase in
370 activation. Given the limited potential benefit of combining gRNA, we kept a narrow focus on
371 testing individual gRNAs alone, though future optimization may include combining guides to
372 increase gene expression. We also performed a post hoc analysis of predicted gRNA efficiency
373 based on insights from CRISPR-editing (Konstantakos et al., 2022). However, based upon the
374 guides screened for this project, as well as additional hcASD target genes that we have studied,
375 we do not find the guidelines for editing efficiency to translate to success in gene activation.
376 Rather, cell type specific characteristics of a particular enhancer are more likely to predict gRNA
377 efficacy (Supplemental Figure 9 and Supplemental Table 1). Nonetheless, the fact that mutant
378 phenotypes were still partially, but significantly, rescued points to the potential for increased
379 phenotypic rescue with increased efficiency.
380 There are potential caveats to the successful clinical application of CRISPR-A. One, as with
381 any therapeutic, there is potential for off-target effects, particularly in highly associated genes. To
382 control for this in our study, we measured the expression of neighboring and closely associated
383 genes to *CHD8* and *SCN2A* and found no increases in expression levels, giving us confidence that
384 our guide RNA constructs were specific to each gene. Second, as both *CHD8* and *SCN2A* vary in
385 their expression across developmental time and are sensitive to overexpression, there is an
386 underlying concern of increasing expression at the relevant period in development. To address
387 this, we focused on enhancers predicted to be specifically active during fetal brain development.
388 Additionally, we applied the CRISPR-A system to mutant organoids at the period of development
389 where CHD8 or SCN2A expression peaked in wildtype organoids. Endogenous gene expression
390 regulation may render the timing of CRISPR-A treatment irrelevant, though an open question
391 remains regarding the effect of introducing CRISPR-A after the expected peak in expression. It is
392 likely that this would vary on a gene-by-gene basis; as *CHD8* is a key regulator of many
393 downstream processes, including many other hcASD genes, late treatment of CRISPR-A may have
394 limited benefit. By contrast, *SCN2A* potentially could be targeted later, since neurons express the
395 sodium channel subunit, and *SCN2A* expression is successively replaced by *SCN8A* as
396 development progresses (Brunklaus & Lal, 2020), which may also contribute to a milder
397 phenotype. Lastly, for genes such as *CHD8*, where gastrointestinal aberrations are a well-
398 characterized patient phenotype, it may be beneficial to consider more generally accessible
399 enhancer regions.
400 Our study also demonstrates the practical application of iPSC-derived cells in modeling
401 neurodevelopmental disorders and testing clinical interventions. Collectively, we provide a
402 workflow that can be adapted to target other hcASD genes and a proof-of-concept for the use of
403 gene activation techniques as a therapeutic intervention for ASD.

Materials and Methods

Guide RNA Design

Putative enhancer regions were identified using data from previously published studies from our lab (de la Torre-Ubieta et al., 2018; Walker et al., 2019; Won et al., 2019). We used the ECR browser (Ovcharenko et al., 2004) to check identified sequences for conservation in the Mus Musculus genome, for the potential use of guides in animal studies. Using the UCSC Genome Browser (Frankish et al., 2018), we focused on sequences within identified regions that corresponded with a DNAse I binding site. The resulting optimized sequences were run through CRISPOR (Concordet & Haeussler, 2018) to design putative guide RNA. One to three top-scoring guide RNA sequences per enhancer were chosen for synthesis.

Golden Gate Assembly

Per guide RNA, “CACCG” was appended to the 5’ end of the sense strand, “AAAC” was appended to the 5’ end of the antisense strand. Single strand DNA oligonucleotides were ligated using T4 Polynucleuotide Kinase (New England Biolabs) using manufacturer instructions. Ligated oligonucleotides were then assembled with pLV-U6-sgRNA using BsmBI (New England Biolabs) and T7 ligase (Thermo). pLV-U6-gRNA-UbC-eGFP-P2A-Bsr was a gift from Charles Gersbach (Addgene plasmid # 83925; http://n2t.net/addgene:83925; RRID:Addgene_83925). Plasmids were transformed into DH5a competent cells (New England Biolabs) on LB agar plates with ampicillin. After overnight culture, single colonies were picked and cultured overnight in Terrific Broth with Ampicillin. Plasmids were purified using a Zymo miniprep kit (Zymo) and sequenced to verify correct insertion.

Cell Culture

HEK293T cells were cultured in DMEM + 10% FBS. For guide RNA screening, 4*10^5 cells per well were seeded into a 12-well tissue culture plate. The next day, cells were transfected with 300ng/well dCas9-p300 plasmid and 200ng gRNA plasmid using Lipofectamine 2000 (Thermo) and incubated for 48 hours. Cells were then collected with Trizol (Thermo) and RNA extracted using a DirectZol RNA miniprep kit (Zymo). cDNA was synthesized from 500ng RNA using a Multiscribe High Capacity cDNA Synthesis kit (Thermo) and qPCR was performed using Luna qPCR Master Mix (New England Biolabs) against primers listed in table 2.

Human Neural Progenitor cells (hNPs) were isolated from discarded tissues as previously published (de la Torre-Ubieta et al., 2018) and cultured on laminin-coated TC plates. For guide RNA screening, 2*10^5 cells per well were plated in 6-well plates. After 24 hours, cells were transduced with lentivirus with 6 ug/ml Polybrene overnight. Media was replaced after overnight incubation and cells were incubated for 72 hours prior to collecting the cells for RNA isolation, cDNA synthesis, and qPCR as described with HEK293T cells.

Stem cells were thawed and plated into 1 well of a 6-well plate coated with vitronectin using E8 media (Thermo). Media was changed daily and cells passaged weekly. The dCas9-p300 line was a generous gift from Dr. Charles Gersbach.

Lentiviral Production

HEK293T cells were plated in 10 cm tissue culture dishes at a density of 3.8*10^5 cells per dish. The next day, cells were transfected with 9ug psPAX2, 900ng pCAG-VSVG, and 9ug plasmid of interest using OptiMEM (Thermo) and Lipofectamine 3000 (Thermo). After 18 hours, cell media was replaced by DMEM + 10% FBS + BSA and harvested every 24 hours for 48 hours. Collected crude virus was concentrated with Lenti-X (Takara Bio) following manufacturer instructions. Titer was determined using Lenti-X qRT-PCR Titration Kit (Takara Bio 631235). pLV-dCas9-p300-P2A-PuroR was a gift from Charles Gersbach (Addgene plasmid # 83889; http://n2t.net/addgene:83889 ; RRID:Addgene_83889). SP-dCas9-VPR was a gift from George Church (Addgene plasmid # 63798; http://n2t.net/addgene:63798 ; RRID:Addgene_63798).

Cortical organoids

Human cortical organoids were produced as previously published (Pasca et al., 2015; Yoon et al., 2019). Briefly, stem cells were seeded into an Aggrewell 800 tissue culture plate (Stem Cell Technologies) at 3*10^6 cells per well in 1.5mL E8 media (Thermo). Every 24 hours for 3 days, media was replaced without disrupting the embryoid bodies in the microwells with E6 media containing 5uM dorsomorphin, 10uM SB431542, and 2.5uM XAV939. On the fourth day, EBs were collected from each well with a wide bore pipette tip and a 40um strainer (Pluriselect) to be plated in 10cm ultralow attachment tissue culture dishes (Corning, Sbio). The culture was undisturbed for the fifth day. After an additional 2 days of culture in E6 media with dorsomorphin, SB431542, and XAV939 with daily changes, the media is changed to Neurobasal A supplemented with B27 without vitamin A (Thermo), GlutaMAX (Thermo), 20ng/ml EGF, and 20ng/ml FGF (NBA + E/F) and replaced daily until day 17 post-initiation. From day 18-25, media is replaced every other day. From day 26-43, the media is replaced every other day with Neurobasal A with B27 without vitamin A, GlutaMAX, 20ng/ml BDNF, and 20ng/ml NT3. After day 43, media is replaced approximately every four days with Neurobasal A with B27 without vitamin A and GlutaMAX.

For organoid infection, three organoids per condition were plated in an ultralow attachment 24-well plate (Corning). Lentivirus was infected at MOI 7 for 24 hours. Organoids were collected post-infection for RNA and imaging. For each application, a minimum of three organoids were combined to create one biological replicate for bulk RNA isolation. Organoids were collected and flash frozen in Trizol. RNA isolation was performed using an Arcteus PicoPure RNA Isolation Kit (Thermo). RNA integrity and concentration was determined using an Agilent Bioanalyzer RNA Pico chip (Agilent). cDNA synthesis was performed using a Multiscribe High-Capacity cDNA synthesis kit (Thermo) or SuperScript IV (Thermo).

Bulk RNA Sequencing

RNA sequencing libraries were prepared using the Ovation RNA Ultralow input kit (Tecan) and sequenced using an Illumina NovaSeq S4 flow cell (PE 2 x 100). Raw reads were trimmed with cutadapt (Martin, 2011) and aligned to hg19 using hisat2. Differential expression analysis was conducted using DESeq2 (Love et al., 2014). Gene Ontology analysis was conducted using clusterProfiler (Wu et al., 2021).

Organoid size measurements

Tissue culture plates were photographed on a lightbox with a metric ruler to standardize measurements between images. Diameter measurements were taken in pixels using Adobe Photoshop, and the volume calculated assuming an ellipsoidal shape.

Neuron differentiation

Stem cells were differentiated to excitatory neurons using NGN2 overexpression as described previously (Zhang et al., 2013). Briefly, stem cell lines were stably transduced to express TetO-Ngn2-Puro and Ubq-rtTA. Cells were plated onto Matrigel-coated 6-well plates at a density of 4*10^5 to 8*10^5 cells/well in pre-differentiation media comprised of Knockout DMEM:F12 with 1x N2 Supplement, 1x non-essential amino acids (NEAA, Thermo), 10ng/ml BDNF, 10ng/ml NT3, 1ug/ml laminin, and 2ug/ml doxycycline. Media was changed daily. After two days in pre-differentiation media, cells were collected and plated onto laminin-coated coverslips or tissue culture wells at a density of 1*10^5-8*10^5 cells/well in maturation media comprised of 50% Neurobasal A, 50% DMEM:F12, 0.5x N2 supplement, 0.5x B27 supplement, 1x NEAA, 0.5x GlutaMAX, 10ng/ml BDNF, 10ng/ml NT3, 1ug/ml laminin, and 2ug/ml doxycycline. This was considered to be day 0 of differentiation. At day 3, half of the media was replaced with fresh maturation media. At day 7, half of the media was replaced again, now without doxycycline. At day 14, half of the media was removed and twice that volume of maturation media was added, for a volume 1.5x the original plating volume. This was repeated at day 21, resulting in a 2x final volume. A third of the media was subsequently replaced weekly until neurons were used for downstream applications.

Immunofluorescence

Organoid sectioning

Organoids were fixed with 4% PFA for 24 hours and rinsed with PBS. Samples were then transferred to a 30% sucrose solution and incubated overnight at 4°C. Using an embedding mold, organoids were enrobed in 1% agarose and cut into 40um sections on a vibratome (Leica).

Immunofluorescence

Organoid sections were blocked in PBS with 5% FBS, 1% BSA, 0.3% Triton-X, and 0.1% sodium azide for 20 minutes at room temperature. Primary antibody was diluted in blocking buffer and the section was incubated overnight at 4C. The next day, the section was washed three times with PBS + 0.1% Tween-20. Secondary antibody was diluted in blocking buffer and the section was incubated in the dark at room temperature on a rocker. After three washes with PBS-T, the section was mounted on a slide using Fluormount with DAPI (Southern Biotech). Antibodies used are listed in Table 3.

Imaging and analysis

Slides were imaged on a Zeiss LSM 900. Whole slide images were captured using an Akoya Phenoimager (Akoya Biosciences). Images were quantified using QuPath (Bankhead et al., 2017). To quantify cells, we first used QuPath's cell detection tool to identify cells based on DAPI staining. Next, single channel classifiers were trained on each fluorophore, using a simple threshold for signal intensity. Classifiers were then run together to identify cells staining positive for multiple markers. The same classifiers were used for all slides in the same experiment.

530

Western blotting

531 532 533 534 535 536 537 538 539 540 541 542 543 544 545 546

Cells or organoids were lysed in RIPA buffer containing Halt protease inhibitor (Thermo) for 30 minutes on ice. Whole cell lysates were centrifuged for 15 minutes at 12,000 g at 4C and the supernatants transferred to new microtubes. Protein concentration was quantified using a Pierce BCA assay (Thermo) following manufacturer's instructions. Lysates were normalized to 10-50ug protein per sample and diluted with RIPA buffer and 5X denaturing loading buffer prior to heating at 95C for 5 minutes. Samples were loaded into Mini-Protean 4-20% TGX precast gel (BioRad) or 3-8% NuPAGE precast gel (Thermo) and run at 100V at 4C for 3 hours. Gels were transferred wet onto nitrocellulose membranes overnight at 25V at 4C for 16 hours. Membranes were blocked with 5% BSA in PBS-Tween for 1 hour at room temperature. Primary antibodies (Table 3) were diluted in blocking buffer and incubated with the membrane overnight at 4C. Blots were subsequently washed three times with PBS-T and incubated in HRP-conjugated secondary antibody diluted in blocking buffer at room temperature for 2 hours. After three additional washes, blots were developed using SuperSignal West Dura ECL (Thermo) and imaged using an Azure Biosystems C600 imager. Images were annotated using Adobe Photoshop and quantified using ImageJ.

547

Flow cytometry

548 549 550 551 552 553 554 555 556 557 558 559 560 561

Organoids were dissociated using a modified protocol from the Worthington Papain Dissociation System (Worthington). Briefly, 5-8 organoids were transferred into 2.5ml of freshly-reconstituted papain in EBSS. The organoids were incubated at 37C on a shaker at 100rpm, initially for 30 minutes, pausing every 15 minutes to manually triturate the sample. After no large clumps remained, the dissociated sample was centrifuged at 300g for 5 minutes. The supernatant was discarded and albumin ovomucoid inhibitor solution added per manufacturer's instructions. Cells were then fixed using 4% paraformaldehyde for 15 minutes at room temperature. Cells were then washed with FACS buffer and counted. Samples were divided into approximately 1*10^6 cells/sample for flow cytometry. If permeabilization was necessary, cells were incubated in 0.1% saponin in HBSS for 15 minutes at RT prior to antibody incubation. Cells were incubated in primary antibody for 1 hour at 4C in the dark (Table 3). If a secondary antibody was necessary, cells were washed twice following primary incubation and incubated in secondary antibody for 1 hour at 4C in the dark. Cells were subsequently washed twice and Sytox added to the final cell suspension.

562 563 564 565

EdU staining were conducted per manufacturer's instructions. Organoids are stained with EdU for 2 hours, then incubated for 48 hours prior to dissociation. Click-IT chemistry is conducted per manufacturer's protocol. Samples were processed on a BD LSR II flow cytometer and data was analyzed using FlowJo (Treestar).

566

Electrophysiology

567 568 569 570 571 572

Neurons were differentiated on laminin-coated coverslips as described above. Coverslips were removed from culture wells and placed in an electrophysiology chamber filled with standard artificial cerebral spinal fluid (ACSF) containing (in mM): 130 NaCl, 3 KCl, 1.25 NaH_2PO4, 26 $NaHCO_3$, 2 $MgCl_2$, 2 $CaCl_2$, and 10 glucose) oxygenated with 95% O_2-5% CO_2 (pH 7.2-7.4, osmolality 290-310 mOsm/L). All recordings were performed at room temperature using an

upright microscope (Olympus BX51WI) equipped with differential interference contrast optics (IR-DIC) and fluorescence imaging. Whole-cell patch clamp recordings in voltage- and current-clamp modes were obtained from cells using a MultiClamp 700B amplifier (Molecular Devices) and the Clampex 10.7 acquisition software. The patch pipette (3–5 MΩ resistance) contained a K-gluconate-based solution comprised of (in mM): 112.5 K-gluconate, 4 NaCl, 17.5 KCl, 0.5 $CaCl_2$, 1 $MgCl_2$, 5 ATP (potassium salt), 1 NaGTP, 5 EGTA, 10 HEPES, pH 7.2 (270–280 mOsm/L). Within 5 min of breaking through the cell membrane, passive membrane properties (capacitance and input resistance) were recorded while holding the membrane potential at -70 mV. Spontaneous postsynaptic currents (SPCs) were recorded in gap-free voltage-clamp mode at -70 mV. RMP and all excitability measurements were recorded in current-clamp mode. Rheobase measurements were obtained by injecting cells with depolarizing current pulses (5 ms) until firing was achieved. Input-output functions as a test for cellular excitability were recorded in response to a 1 sec duration depolarizing current injection. All recordings were filtered at 1-2 kHz and digitized at 100 µs. Electrode access resistances during whole-cell recordings were maintained at <30 and recordings obtained with access resistances above 30 MΩ were excluded from analysis.

Acknowledgements

The authors would like to thank the members of the Geschwind lab for their valuable feedback, Dr. Charlie Gersbach and Lexi Bounds for providing the dCas9-p300 construct and lines. We additionally would like to thank the UCLA Neuroscience Genomics Core and UCLA Broad Stem Cell Research Center Flow Cytometry Core for their expertise.

Credits

GTC and DHG conceived the study, designed the experiments, and wrote the manuscript. CL and NES developed and characterized isogenic $CHD8^{+/-}$ and $SCN2A^{+/-}$ cell lines. GTC, GN, and AO characterized the mutant iPSC lines and established hCO cultures. GTC, GN, and AO performed immunofluorescence, microscopy, and image analysis of organoids. GTC and AO performed organoid dissociation and flow cytometry. GTC and KG performed Western blots. GTC and KG designed the guide RNA. GTC, GN, KG, and JG screened the gRNA in HEK293T and hNPCs. GN screened the gRNA in dCas9-p300 cortical organoids. GN and AO treated mutant hCO with CRISPR-A. GTC, GN, AO, and KG performed qPCR analysis on CRISPR-A treated hCO. GTC, GN, and AO differentiated mutant lines into neurons. SH and CC conducted the patch clamp assays and analysis.

Funding

This research was supported by NIH grants to DHG (NIMH R01MH10027, U01MH116489, RM1MH132651), a pilot grant from the Simons Foundation Autism Research Initiative (SFARI), a UCLA Broad Stem Cell Research Center Innovation Award, and a NIH grant to GTC (NIMH F32MH124337). NES is supported by the Simons Foundation Autism Research Initiative (Genomics of ASD 896724). Electrophysiology experiments were supported by the Cell, Circuits and Systems Analysis Core (NIH P50HD103557).

611 ## References

612 Bankhead, P., Loughrey, M. B., Fernández, J. A., Dombrowski, Y., McArt, D. G., Dunne, P. D.,
613 McQuaid, S., Gray, R. T., Murray, L. J., Coleman, H. G., James, J. A., Salto-Tellez, M., &
614 Hamilton, P. W. (2017). QuPath: Open source software for digital pathology image
615 analysis. *Scientific Reports*, *7*(1), 1–7. https://doi.org/10.1038/s41598-017-17204-5

616 Ben-Shalom, R., Keeshen, C. M., Berrios, K. N., An, J. Y., Sanders, S. J., & Bender, K. J. (2017).
617 Opposing Effects on NaV1.2 Function Underlie Differences Between SCN2A Variants
618 Observed in Individuals With Autism Spectrum Disorder or Infantile Seizures. *Biological*
619 *Psychiatry*, *82*(3), 224–232. https://doi.org/10.1016/j.biopsych.2017.01.009

620 Bernier, R., Golzio, C., Xiong, B., Stessman, H. A., Coe, B. P., Penn, O., Witherspoon, K., Gerdts, J.,
621 Baker, C., Vulto-Van Silfhout, A. T., Schuurs-Hoeijmakers, J. H., Fichera, M., Bosco, P.,
622 Buono, S., Alberti, A., Failla, P., Peeters, H., Steyaert, J., Vissers, L. E. L. M., … Eichler, E. E.
623 (2014). Disruptive CHD8 mutations define a subtype of autism early in development.
624 *Cell*, *158*(2), 263–276. https://doi.org/10.1016/j.cell.2014.06.017

625 Brunklaus, A., & Lal, D. (2020). Sodium channel epilepsies and neurodevelopmental disorders:
626 From disease mechanisms to clinical application. *Developmental Medicine and Child*
627 *Neurology*, *62*(7), 784–792. https://doi.org/10.1111/dmcn.14519

628 Chen, G. T., & Geschwind, D. H. (2022). Challenges and opportunities for precision medicine in
629 neurodevelopmental disorders. *Advanced Drug Delivery Reviews*, *191*, 114564.
630 https://doi.org/10.1016/j.addr.2022.114564

631 Cirnigliaro, M., Chang, T. S., Arteaga, S. A., Pérez-Cano, L., Ruzzo, E. K., Gordon, A., Bicks, L. K.,
632 Jung, J.-Y., Lowe, J. K., Wall, D. P., & Geschwind, D. H. (2023). The contributions of rare

633 inherited and polygenic risk to ASD in multiplex families. *Proceedings of the National*
634 *Academy of Sciences*, *120*(31), e2215632120. https://doi.org/10.1073/pnas.2215632120
635 Colasante, G., Lignani, G., Brusco, S., Di Berardino, C., Carpenter, J., Giannelli, S., Valassina, N.,
636 Bido, S., Ricci, R., Castoldi, V., Marenna, S., Church, T., Massimino, L., Morabito, G.,
637 Benfenati, F., Schorge, S., Leocani, L., Kullmann, D. M., & Broccoli, V. (2019). dCas9-Based
638 Scn1a Gene Activation Restores Inhibitory Interneuron Excitability and Attenuates
639 Seizures in Dravet Syndrome Mice. *Molecular Therapy*, *28*(1), 235–253.
640 https://doi.org/10.1016/j.ymthe.2019.08.018
641 Colasante, G., Qiu, Y., Massimino, L., Di Berardino, C., Cornford, J. H., Snowball, A., Weston, M.,
642 Jones, S. P., Giannelli, S., Lieb, A., Schorge, S., Kullmann, D. M., Broccoli, V., & Lignani, G.
643 (2020). In vivo CRISPRa decreases seizures and rescues cognitive deficits in a rodent
644 model of epilepsy. *Brain*, *143*(3), 891–905. https://doi.org/10.1093/brain/awaa045
645 Collins, R. L., Brand, H., Karczewski, K. J., Zhao, X., Alföldi, J., Francioli, L. C., Khera, A. V., Lowther,
646 C., Gauthier, L. D., Wang, H., Watts, N. A., Solomonson, M., O'Donnell-Luria, A.,
647 Baumann, A., Munshi, R., Walker, M., Whelan, C. W., Huang, Y., Brookings, T., …
648 Talkowski, M. E. (2020). A structural variation reference for medical and population
649 genetics. *Nature*, *581*(7809), 444–451. https://doi.org/10.1038/s41586-020-2287-8
650 Collins, R. L., Glessner, J. T., Porcu, E., Lepamets, M., Brandon, R., Lauricella, C., Han, L., Morley,
651 T., Niestroj, L.-M., Ulirsch, J., Everett, S., Howrigan, D. P., Boone, P. M., Fu, J., Karczewski,
652 K. J., Kellaris, G., Lowther, C., Lucente, D., Mohajeri, K., … Esko, T. (2022). A cross-disorder
653 dosage sensitivity map of the human genome. *Cell*, *185*(16), 3041-3055.e25.
654 https://doi.org/10.1016/j.cell.2022.06.036

Concordet, J.-P., & Haeussler, M. (2018). CRISPOR: intuitive guide selection for CRISPR/Cas9 genome editing experiments and screens. *Nucleic Acids Research*, *46*(W1), W242–W245. https://doi.org/10.1093/nar/gky354

de la Torre-Ubieta, L., Stein, J. L., Won, H., Opland, C. K., Liang, D., Lu, D., & Geschwind, D. H. (2018). The Dynamic Landscape of Open Chromatin during Human Cortical Neurogenesis. *Cell*, *172*(1–2), 289-304.e18. https://doi.org/10.1016/j.cell.2017.12.014

de la Torre-Ubieta, L., Won, H., Stein, J. L., & Geschwind, D. H. (2016). Advancing the understanding of autism disease mechanisms through genetics. *Nature Medicine*, *22*(4), 345–361. https://doi.org/10.1038/nm.4071

Eaton, M., Zhang, J., Ma, Z., Park, A. C., Lietzke, E., Romero, C. M., Liu, Y., Coleman, E. R., Chen, X., Xiao, T., Que, Z., Lai, S., Wu, J., Lee, J. H., Palant, S., Nguyen, H. P., Huang, Z., Skarnes, W. C., Koss, W. A., & Yang, Y. (2021). Generation and basic characterization of a gene-trap knockout mouse model of *Scn2a* with a substantial reduction of voltage-gated sodium channel Na_v 1.2 expression. *Genes, Brain and Behavior*, *20*(4), e12725. https://doi.org/10.1111/gbb.12725

Frankish, A., Diekhans, M., Ferreira, A.-M., Johnson, R., Jungreis, I., Loveland, J., Mudge, J. M., Sisu, C., Wright, J., Armstrong, J., Barnes, I., Berry, A., Bignell, A., Carbonell Sala, S., Chrast, J., Cunningham, F., Di Domenico, T., Donaldson, S., Fiddes, I. T., … Flicek, P. (2018). GENCODE reference annotation for the human and mouse genomes. *Nucleic Acids Research*, *47*(October 2018), 766–773. https://doi.org/10.1093/nar/gky955

Fu, J. M., Satterstrom, F. K., Peng, M., Brand, H., Collins, R. L., Dong, S., Wamsley, B., Klei, L., Wang, L., Hao, S. P., Stevens, C. R., Cusick, C., Babadi, M., Banks, E., Collins, B., Dodge, S.,

Gabriel, S. B., Gauthier, L., Lee, S. K., … Talkowski, M. E. (2022). Rare coding variation provides insight into the genetic architecture and phenotypic context of autism. *Nature Genetics*, *54*(9), 1320–1331. https://doi.org/10.1038/s41588-022-01104-0

Gaugler, T., Klei, L., Sanders, S. J., Bodea, C. A., Goldberg, A. P., Lee, A. B., Mahajan, M., Manaa, D., Pawitan, Y., Reichert, J., Ripke, S., Sandin, S., Sklar, P., Svantesson, O., Reichenberg, A., Hultman, C. M., Devlin, B., Roeder, K., & Buxbaum, J. D. (2014). Most genetic risk for autism resides with common variation. *Nature Genetics*, *46*(8), 881–885. https://doi.org/10.1038/ng.3039

Geschwind, D. H., & State, M. W. (2015). Gene hunting in autism spectrum disorder: On the path to precision medicine. *The Lancet Neurology*, *14*(11), 1109–1120. https://doi.org/10.1016/S1474-4422(15)00044-7

Gompers, A. L., Su-Feher, L., Ellegood, J., Copping, N. A., Riyadh, M. A., Stradleigh, T. W., Pride, M. C., Schaffler, M. D., Wade, A. A., Catta-Preta, R., Zdilar, I., Louis, S., Kaushik, G., Mannion, B. J., Plajzer-Frick, I., Afzal, V., Visel, A., Pennacchio, L. A., Dickel, D. E., … Nord, A. S. (2017). Germline Chd8 haploinsufficiency alters brain development in mouse. *Nature Neuroscience*, *20*(8), 1062–1073. https://doi.org/10.1038/nn.4592

Gordon, A., Yoon, S., Tran, S. S., Makinson, C. D., Park, J. Y., Andersen, J., Valencia, A. M., Horvath, S., Xiao, X., Huguenard, J. R., Pașca, S. P., & Geschwind, D. H. (2021). Long-term maturation of human cortical organoids matches key early postnatal transitions. *Nature Neuroscience*, *24*(3), 331–342. https://doi.org/10.1038/s41593-021-00802-y

Hilton, I. B., D'Ippolito, A. M., Vockley, C. M., Thakore, P. I., Crawford, G. E., Reddy, T. E., & Gersbach, C. A. (2015). Epigenome editing by a CRISPR-Cas9-based acetyltransferase

activates genes from promoters and enhancers. *Nature Biotechnology*, *33*(5), 510–517. https://doi.org/10.1038/nbt.3199

Huang, N., Lee, I., Marcotte, E. M., & Hurles, M. E. (2010). Characterising and Predicting Haploinsufficiency in the Human Genome. *PLoS Genetics*, *6*(10), e1001154. https://doi.org/10.1371/journal.pgen.1001154

Huang, T. N., Chuang, H. C., Chou, W. H., Chen, C. Y., Wang, H. F., Chou, S. J., & Hsueh, Y. P. (2014). Tbr1 haploinsufficiency impairs amygdalar axonal projections and results in cognitive abnormality. *Nature Neuroscience*, *17*(2), 240–247. https://doi.org/10.1038/nn.3626

Iossifov, I., O'Roak, B. J., Sanders, S. J., Ronemus, M., Krumm, N., Levy, D., Stessman, H. A., Witherspoon, K. T., Vives, L., Patterson, K. E., Smith, J. D., Paeper, B., Nickerson, D. A., Dea, J., Dong, S., Gonzalez, L. E., Mandell, J. D., Mane, S. M., Murtha, M. T., … Wigler, M. (2014). The contribution of de novo coding mutations to autism spectrum disorder. *Nature*, *515*(7526), 216–221. https://doi.org/10.1038/nature13908

Knott, G. J., & Doudna, J. A. (2018). CRISPR-Cas guides the future of genetic engineering. *Science*, *361*(6405), 866–869. https://doi.org/10.1126/science.aat5011

Konstantakos, V., Nentidis, A., Krithara, A., & Paliouras, G. (2022). CRISPR–Cas9 gRNA efficiency prediction: An overview of predictive tools and the role of deep learning. *Nucleic Acids Research*, *50*(7), 3616–3637. https://doi.org/10.1093/nar/gkac192

Lek, M., Karczewski, K. J., Minikel, E. V., Samocha, K. E., Banks, E., Fennell, T., O'Donnell-Luria, A. H., Ware, J. S., Hill, A. J., Cummings, B. B., Tukiainen, T., Birnbaum, D. P., Kosmicki, J. A., Duncan, L. E., Estrada, K., Zhao, F., Zou, J., Pierce-Hoffman, E., Berghout, J., … Williams, A.

L. (2016). Analysis of protein-coding genetic variation in 60,706 humans. *Nature*, *536*(7616), 285–291. https://doi.org/10.1038/nature19057

Love, M. I., Huber, W., & Anders, S. (2014). Moderated estimation of fold change and dispersion for RNA-seq data with DESeq2. *Genome Biology*, *15*(12), 550. https://doi.org/10.1186/s13059-014-0550-8

Lu, C., Shi, X., Allen, A., Baez-Nieto, D., Nikish, A., Sanjana, N. E., & Pan, J. Q. (2019). Overexpression of NEUROG2 and NEUROG1 in human embryonic stem cells produces a network of excitatory and inhibitory neurons. *The FASEB Journal*, *33*(4), 5287–5299. https://doi.org/10.1096/fj.201801110RR

Maenner, M. J., Shaw, K. A., Baio, J., Washington, A., Patrick, M., DiRienzo, M., Christensen, D. L., Wiggins, L. D., Pettygrove, S., Andrews, J. G., Lopez, M., Hudson, A., Baroud, T., Schwenk, Y., White, T., Rosenberg, C. R., Lee, L.-C., Harrington, R. A., Huston, M., … Dietz, P. M. (2020). Prevalence of Autism Spectrum Disorder Among Children Aged 8 Years—Autism and Developmental Disabilities Monitoring Network, 11 Sites, United States, 2016. *MMWR. Surveillance Summaries*, *69*(4), 1–12. https://doi.org/10.15585/mmwr.ss6904a1

Martin, M. (2011). Cutadapt removes adapter sequences from high-throughput sequencing reads. *EMBnet.Journal; Vol 17, No 1: Next Generation Sequencing Data Analysis*. https://doi.org/10.14806/ej.17.1.200

Matharu, N., Rattanasopha, S., Tamura, S., Maliskova, L., Wang, Y., Bernard, A., Hardin, A., Eckalbar, W. L., Vaisse, C., & Ahituv, N. (2018). CRISPR-mediated activation of a promoter or enhancer rescues obesity caused by haploinsufficiency. *Science*, *0629*(December), eaau0629. https://doi.org/10.1126/SCIENCE.AAU0629

Morrill, S. A., & Amon, A. (2019). Why haploinsufficiency persists. *Proceedings of the National Academy of Sciences*, *116*(24), 201900437. https://doi.org/10.1073/pnas.1900437116

Ovcharenko, I., Nobrega, M. A., Loots, G. G., & Stubbs, L. (2004). ECR Browser: A tool for visualizing and accessing data from comparisons of multiple vertebrate genomes. *Nucleic Acids Research*, *32*(WEB SERVER ISS.), 280–286. https://doi.org/10.1093/nar/gkh355

Parikshak, N. N., Luo, R., Zhang, A., Won, H., Lowe, J. K., Chandran, V., Horvath, S., & Geschwind, D. H. (2013). Integrative Functional Genomic Analyses Implicate Specific Molecular Pathways and Circuits in Autism. *Cell*, *155*(5), 1008–1021. https://doi.org/10.1016/j.cell.2013.10.031

Pasca, A. M., Sloan, S. A., Clarke, L. E., Tian, Y., Makinson, C. D., Huber, N., Kim, C. H., Park, J. Y., O'Rourke, N. A., Nguyen, K. D., Smith, S. J., Huguenard, J. R., Geschwind, D. H., Barres, B. A., & Pasca, S. P. (2015). Functional cortical neurons and astrocytes from human pluripotent stem cells in 3D culture. *Nature Methods*, *12*(7), 671–678. https://doi.org/10.1038/nmeth.3415

Pașca, S. P., Arlotta, P., Bateup, H. S., Camp, J. G., Cappello, S., Gage, F. H., Knoblich, J. A., Kriegstein, A. R., Lancaster, M. A., Ming, G., Muotri, A. R., Park, I., Reiner, O., Song, H., Studer, L., Temple, S., Testa, G., Treutlein, B., & Vaccarino, F. M. (2022). *A nomenclature consensus for nervous system organoids and assembloids*. *609*(January), 907–910. https://doi.org/10.1038/s41586-022-05219-6

Paulsen, B., Velasco, S., Kedaigle, A. J., Pigoni, M., Quadrato, G., Deo, A., Adiconis, X., Uzquiano, A., Kim, K., Simmons, S. K., Tsafou, K., Albanese, A., Sartore, R., Abbate, C., Tucewicz, A.,

765 Smith, S., Chung, K., Lage, K., Regev, A., … Arlotta, P. (2020). Human brain organoids
766 reveal accelerated development of cortical neuron classes as a shared feature of autism
767 risk genes. *bioRxiv*, 2020.11.10.376509.
768 Paulsen, B., Velasco, S., Kedaigle, A. J., Pigoni, M., Quadrato, G., Deo, A. J., Adiconis, X.,
769 Uzquiano, A., Sartore, R., Yang, S. M., Simmons, S. K., Symvoulidis, P., Kim, K., Tsafou, K.,
770 Podury, A., Abbate, C., Tucewicz, A., Smith, S. N., Albanese, A., … Arlotta, P. (2022).
771 Autism genes converge on asynchronous development of shared neuron classes. *Nature*,
772 *602*(February). https://doi.org/10.1038/s41586-021-04358-6
773 Platt, R. J., Zhou, Y., Slaymaker, I. M., Shetty, A. S., Weisbach, N. R., Kim, J.-A., Sharma, J., Desai,
774 M., Sood, S., Kempton, H. R., Crabtree, G. R., Feng, G., & Zhang, F. (2017). Chd8 Mutation
775 Leads to Autistic-like Behaviors and Impaired Striatal Circuits. *Cell Reports*, *19*(2), 335–
776 350. https://doi.org/10.1016/j.celrep.2017.03.052
777 Ricci, R., & Colasante, G. (2021). CRISPR/dCas9 as a Therapeutic Approach for
778 Neurodevelopmental Disorders: Innovations and Limitations Compared to Traditional
779 Strategies. *Developmental Neuroscience*, *43*(3), 253–261.
780 https://doi.org/10.1159/000515845
781 Rolland, T., Cliquet, F., Anney, R. J. L., Moreau, C., Traut, N., Mathieu, A., Huguet, G., Duan, J.,
782 Warrier, V., Portalier, S., Dry, L., Leblond, C. S., Douard, E., Amsellem, F., Malesys, S.,
783 Maruani, A., Toro, R., Børglum, A. D., Grove, J., … Bourgeron, T. (2023). Phenotypic
784 effects of genetic variants associated with autism. *Nature Medicine*, *29*(7), 1671–1680.
785 https://doi.org/10.1038/s41591-023-02408-2

Ronemus, M., Iossifov, I., Levy, D., & Wigler, M. (2014). The role of de novo mutations in the genetics of autism spectrum disorders. *Nature Reviews Genetics*, *15*(2), 133–141. https://doi.org/10.1038/nrg3585

Ruzzo, E. K., Pérez-Cano, L., Jung, J.-Y., Wang, L., Kashef-Haghighi, D., Hartl, C., Singh, C., Xu, J., Hoekstra, J. N., Leventhal, O., Leppä, V. M., Gandal, M. J., Paskov, K., Stockham, N., Polioudakis, D., Lowe, J. K., Prober, D. A., Geschwind, D. H., & Wall, D. P. (2019). Inherited and De Novo Genetic Risk for Autism Impacts Shared Networks. *Cell*, *178*(4), 850-866.e26. https://doi.org/10.1016/j.cell.2019.07.015

Sahin, M., & Sur, M. (2015). Genes, circuits, and precision therapies for autism and related neurodevelopmental disorders. *Science*, *350*(6263), 1–8. https://doi.org/10.1126/science.aab3897

Sanders, S. J., Murtha, M. T., Gupta, A. R., Murdoch, J. D., Raubeson, M. J., Willsey, A. J., Ercan-Sencicek, A. G., DiLullo, N. M., Parikshak, N. N., Stein, J. L., Walker, M. F., Ober, G. T., Teran, N. A., Song, Y., El-Fishawy, P., Murtha, R. C., Choi, M., Overton, J. D., Bjornson, R. D., … State, M. W. (2012). De novo mutations revealed by whole-exome sequencing are strongly associated with autism. *Nature*, *485*(7397), 237–241. https://doi.org/10.1038/nature10945

Satterstrom, F. K., Kosmicki, J. A., Wang, J., Breen, M. S., De Rubeis, S., An, J.-Y., Peng, M., Collins, R., Grove, J., Klei, L., Stevens, C., Reichert, J., Mulhern, M. S., Artomov, M., Gerges, S., Sheppard, B., Xu, X., Bhaduri, A., Norman, U., … Walters, R. K. (2020). Large-Scale Exome Sequencing Study Implicates Both Developmental and Functional Changes in the

Neurobiology of Autism. *Cell*, *180*(3), 568-584.e23. https://doi.org/10.1016/j.cell.2019.12.036

Savell, K. E., Bach, S. V., Zipperly, M. E., Revanna, J. S., Goska, N. A., Tuscher, J. J., Duke, C. G., Sultan, F. A., Burke, J. N., Williams, D. M., Ianov, L., & Day, J. J. (2018). A neuron-optimized CRISPR/dCas9 activation system for robust and specific gene regulation. *bioRxiv*, 371500. https://doi.org/10.1101/371500

Schafer, S. T., Paquola, A. C. M., Stern, S., Gosselin, D., Ku, M., Pena, M., Kuret, T. J. M., Liyanage, M., Mansour, A. A. F., Jaeger, B. N., Marchetto, M. C., Glass, C. K., Mertens, J., & Gage, F. H. (2019). Pathological priming causes developmental gene network heterochronicity in autistic subject-derived neurons. *Nature Neuroscience*, *22*(2), 243–255. https://doi.org/10.1038/s41593-018-0295-x

Shi, X., Lu, C., Corman, A., Nikish, A., Zhou, Y., Platt, R. J., Iossifov, I., Zhang, F., Pan, J. Q., & Sanjana, N. E. (2023). Heterozygous deletion of the autism-associated gene CHD8 impairs synaptic function through widespread changes in gene expression and chromatin compaction. *The American Journal of Human Genetics*, *110*(10), 1750–1768. https://doi.org/10.1016/j.ajhg.2023.09.004

Spratt, P. W. E., Ben-Shalom, R., Keeshen, C. M., Burke, K. J., Clarkson, R. L., Sanders, S. J., & Bender, K. J. (2019). The Autism-Associated Gene Scn2a Contributes to Dendritic Excitability and Synaptic Function in the Prefrontal Cortex. *Neuron*, *103*(4), 673-685.e5. https://doi.org/10.1016/j.neuron.2019.05.037

Tamura, S., Nelson, A. D., Spratt, P. W. E., Kyoung, H., Zhou, X., Li, Z., Zhao, J., Holden, S. S., Sahagun, A., Keeshen, C. M., Lu, C., Hamada, E. C., Ben-Shalom, R., Pan, J. Q., Paz, J. T.,

Sanders, S. J., Matharu, N., Ahituv, N., & Bender, K. J. (2022). CRISPR activation rescues abnormalities in *SCN2A* haploinsufficiency-associated autism spectrum disorder. *BioRxiv*. https://doi.org/10.1101/2022.03.30.486483

Tatsukawa, T., Raveau, M., Ogiwara, I., Hattori, S., Miyamoto, H., Mazaki, E., Itohara, S., Miyakawa, T., Montal, M., & Yamakawa, K. (2019). Scn2a haploinsufficient mice display a spectrum of phenotypes affecting anxiety, sociability, memory flexibility and ampakine CX516 rescues their hyperactivity. *Molecular Autism*, *10*(1), 1–15. https://doi.org/10.1186/s13229-019-0265-5

Veitia, R. A., & Potier, M. C. (2015). Gene dosage imbalances: Action, reaction, and models. *Trends in Biochemical Sciences*, *40*(6), 309–317. https://doi.org/10.1016/j.tibs.2015.03.011

Villa, C. E., Cheroni, C., Tóbon, A. L.-, Dotter, C. P., Oliveira, B., Sacco, R., Yahya, A. C., Morandell, J., Gabriele, M., Sommer, C., Gabitto, M., Testa1, G., & Novarino, G. (2020). CHD8 haploinsufficiency alters the developmental trajectories of human excitatory and inhibitory neurons linking autism phenotypes with transient cellular defects. *bioRxiv*, *8*, 1–37. https://doi.org/10.1101/2020.11.26.399469

Vorstman, J. A. S., & Scherer, S. W. (2023). Contemplating syndromic autism. *Genetics in Medicine*, *25*(10), 100919. https://doi.org/10.1016/j.gim.2023.100919

Walker, R. L., Ramaswami, G., Hartl, C., Mancuso, N., Michael, J., Torre-ubieta, L. D., Pasaniuc, B., Stein, J. L., Daniel, H., Gandal, M. J., de la Torre-Ubieta, L., Pasaniuc, B., Stein, J. L., & Geschwind, D. H. (2019). Genetic Control of Expression and Splicing in Developing

Human Brain Informs Disease Mechanisms. *Cell*, *179*(3), 750-771.e22. https://doi.org/10.1016/j.cell.2019.09.021

Wang, D., Liu, S., Warrell, J., Won, H., Shi, X., Navarro, F. C. P., Clarke, D., Gu, M., Emani, P., Yang, Y. T., Xu, M., Gandal, M. J., Lou, S., Zhang, J., Park, J. J., Yan, C., Rhie, S. K., Manakongtreecheep, K., Zhou, H., … Gerstein, M. B. (2018). Comprehensive functional genomic resource and integrative model for the human brain. *Science*, *362*(6420), eaat8464. https://doi.org/10.1126/science.aat8464

Wang, P., Mokhtari, R., Pedrosa, E., Kirschenbaum, M., Bayrak, C., Zheng, D., & Lachman, H. M. (2017). CRISPR/Cas9-mediated heterozygous knockout of the autism gene CHD8 and characterization of its transcriptional networks in cerebral organoids derived from iPS cells. *Molecular Autism*, *8*(1), 1–17. https://doi.org/10.1186/s13229-017-0124-1

Weuring, W., Geerligs, J., & Koeleman, B. P. C. (2021). *Gene Therapies for Monogenic Autism Spectrum Disorders*.

Whiteley, J. T., Fernandes, S., Sharma, A., Mendes, A. P. D., Racha, V., Benassi, S. K., & Marchetto, M. C. (2022). Reaching into the toolbox: Stem cell models to study neuropsychiatric disorders. *Stem Cell Reports*, *17*(2), 187–210. https://doi.org/10.1016/j.stemcr.2021.12.015

Wolff, M., Johannesen, K. M., Hedrich, U. B. S., Masnada, S., Rubboli, G., Gardella, E., Lesca, G., Ville, D., Milh, M., Villard, L., Afenjar, A., Chantot-Bastaraud, S., Mignot, C., Lardennois, C., Nava, C., Schwarz, N., Gérard, M., Perrin, L., Doummar, D., … Møller, R. S. (2017). Genetic and phenotypic heterogeneity suggest therapeutic implications in SCN2A-related disorders. *Brain*, *140*(5), 1316–1336. https://doi.org/10.1093/brain/awx054

Won, H., De La Torre-Ubieta, L., Stein, J. L., Parikshak, N. N., Huang, J., Opland, C. K., Gandal, M. J., Sutton, G. J., Hormozdiari, F., Lu, D., Lee, C., Eskin, E., Voineagu, I., Ernst, J., & Geschwind, D. H. (2016). Chromosome conformation elucidates regulatory relationships in developing human brain. *Nature*, *538*(7626), 523–527. https://doi.org/10.1038/nature19847

Won, H., Huang, J., Opland, C. K., Hartl, C. L., & Geschwind, D. H. (2019). Human evolved regulatory elements modulate genes involved in cortical expansion and neurodevelopmental disease susceptibility. *Nature Communications*, *10*(1), 1–11. https://doi.org/10.1038/s41467-019-10248-3

Wu, T., Hu, E., Xu, S., Chen, M., Guo, P., Dai, Z., Feng, T., Zhou, L., Tang, W., Zhan, L., Fu, X., Liu, S., Bo, X., & Yu, G. (2021). clusterProfiler 4.0: A universal enrichment tool for interpreting omics data. *The Innovation*, *2*(3), 100141. https://doi.org/10.1016/j.xinn.2021.100141

Yang, Y., Wu, J., Zhang, J., Chen, X., Que, Z., Wettschurack, K., Deming, B., Acosta, M., Cui, N., Eaton, M., Zhao, Y., Halurkar, M., Purba, M., Chen, I., Xiao, T., Suzuki, M., Yuan, C., Xu, R., Koss, W., … Wu, L.-J. (2023). *Microglial over-pruning of synapses during development in autism-associated SCN2A-deficient mice and human cerebral organoids* [Preprint]. In Review. https://doi.org/10.21203/rs.3.rs-3270664/v1

Yoon, S.-J., Elahi, L. S., Pașca, A. M., Marton, R. M., Gordon, A., Revah, O., Miura, Y., Walczak, E. M., Holdgate, G. M., Fan, H. C., Huguenard, J. R., Geschwind, D. H., & Pașca, S. P. (2019). Reliability of human cortical organoid generation. *Nature Methods*, *16*(1), 75–78. https://doi.org/10.1038/s41592-018-0255-0

Zhang, Y., Pak, C., Han, Y., Ahlenius, H., Zhang, Z., Chanda, S., Marro, S., Patzke, C., Acuna, C., Covy, J., Xu, W., Yang, N., Danko, T., Chen, L., Wernig, M., & Südhof, T. C. (2013). Rapid Single-Step Induction of Functional Neurons from Human Pluripotent Stem Cells. *Neuron*, *78*(5), 785–798. https://doi.org/10.1016/j.neuron.2013.05.029

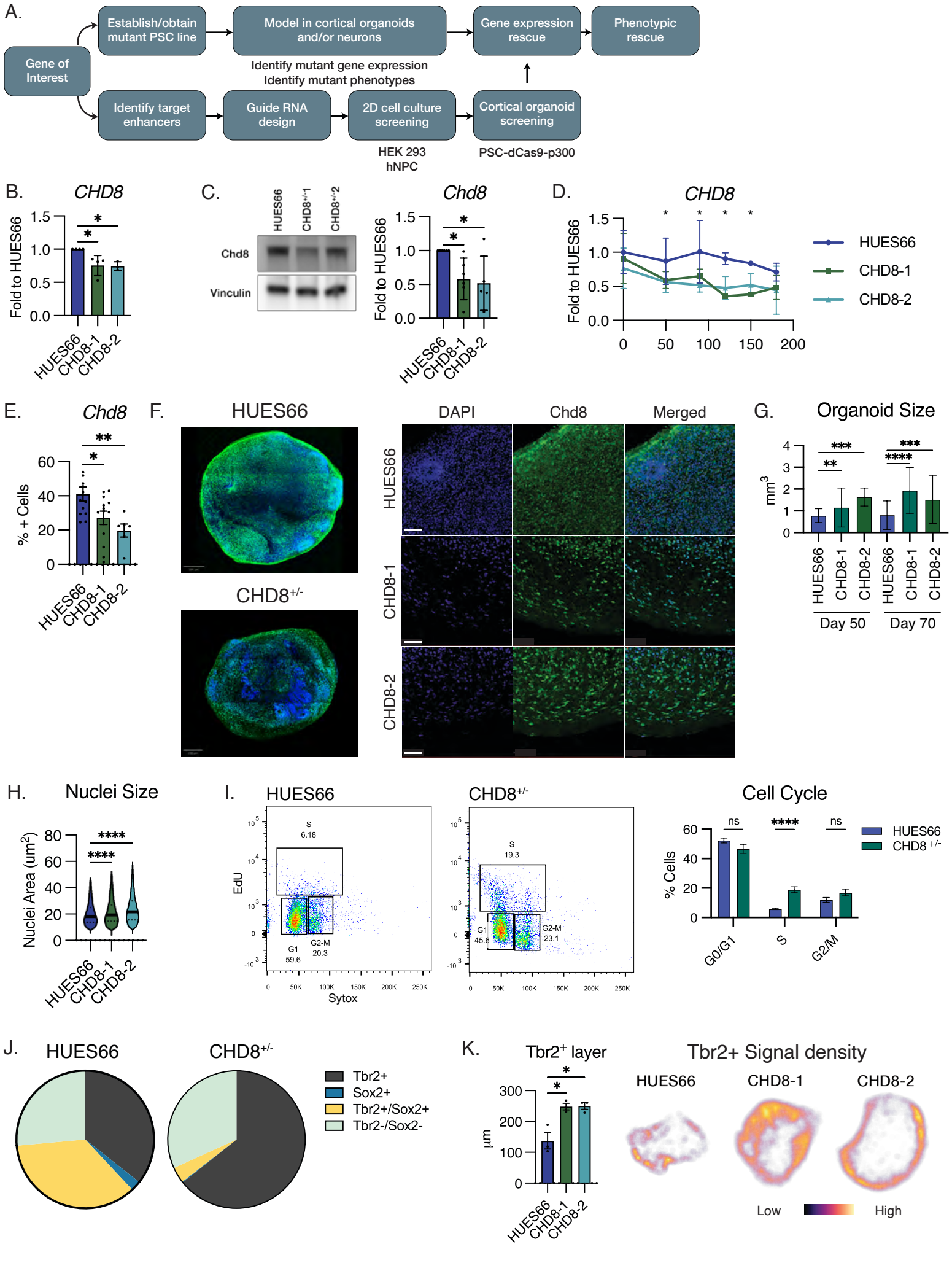
A.
Gene of Interest
Establish/obtain mutant PSC line
Model in cortical organoids and/or neurons
Gene expression rescue
Phenotypic rescue
Identify mutant gene expression
Identify mutant phenotypes
Identify target enhancers
Guide RNA design
2D cell culture screening
Cortical organoid screening
HEK 293
hNPC
PSC-dCas9-p300
B.
CHD8
Fold to HUES66
HUES66
CHD8-1
CHD8-2
C.
HUES66
CHD8+/-1
CHD8+/-2
Chd8
Vinculin
Chd8
Fold to HUES66
D.
CHD8
Fold to HUES66
HUES66
CHD8-1
CHD8-2
E.
Chd8
% + Cells
F.
HUES66
CHD8+/-
DAPI
Chd8
Merged
G.
Organoid Size
mm3
Day 50
Day 70
H.
Nuclei Size
Nuclei Area (um2)
I.
HUES66
CHD8+/-
EdU
Sytox
Cell Cycle
% Cells
G0/G1
S
G2/M
ns
****
J.
HUES66
CHD8+/-
Tbr2+
Sox2+
Tbr2+/Sox2+
Tbr2-/Sox2-
K.
Tbr2+ layer
µm
Tbr2+ Signal density
Low
High

Figure 1. Characterization of CHD8 mutant stem cells and organoids. (A) Overview of workflow for each gene of interest. (B) RNA expression of CHD8 shows expected 50% reduction in mutant lines compared to wildtype control. N = 4, SD shown, * $p < 0.05$. (C) Protein expression of CHD8 shows a 50% reduction in mutant lines compared to wildtype control. N = 6, SD shown, * $p < 0.05$. (D) Expression of CHD8 in cortical organoids from day 0 to 180 shows a consistently lower level of CHD8 across all timepoints measured. N = 6, SEM shown. (E-F) immunofluorescence of Chd8 in 90-day old organoid sections shows lower levels of Chd8 in mutant organoids, quantified in (E). N = 7, SD shown, * $p < 0.05$. (G) Organoid size measurements in 50- and 70-day old cortical organoids show CHD8-mutant organoids (CHD8-1, CHD8-2) are significantly larger than wildtype (H66). N = 120, SD shown. (H) Nuclei size of cells in organoid sections shows significantly larger nuclei in $CHD8^{+/-}$ organoids. N = 120, * $p < 0.05$. (I) Flow cytometry of EdU- and Sytox-stained organoids shows an increase in cell proliferation in CHD8 organoids. Quantitation of cell cycle state shows a significant difference in proportion of $CHD8^{+/-}$ cells in S phase compared to HUES66 cells at matching timepoints. N = 9, SD shown, * $p < 0.05$. (J) Expression of cell type markers Tbr2 and Sox2 in $CHD8^{+/-}$ and Control organoids shows a larger proportion of Tbr2+ cells in mutant organoids. (K) Tbr2+ area in organoid sections shows an expanded Tbr2+ layer thickness in CHD8-mutant organoids. N = 3, * $p < 0.05$. Sample density maps of organoid sections; brighter colors indicate higher Tbr2+ signal.

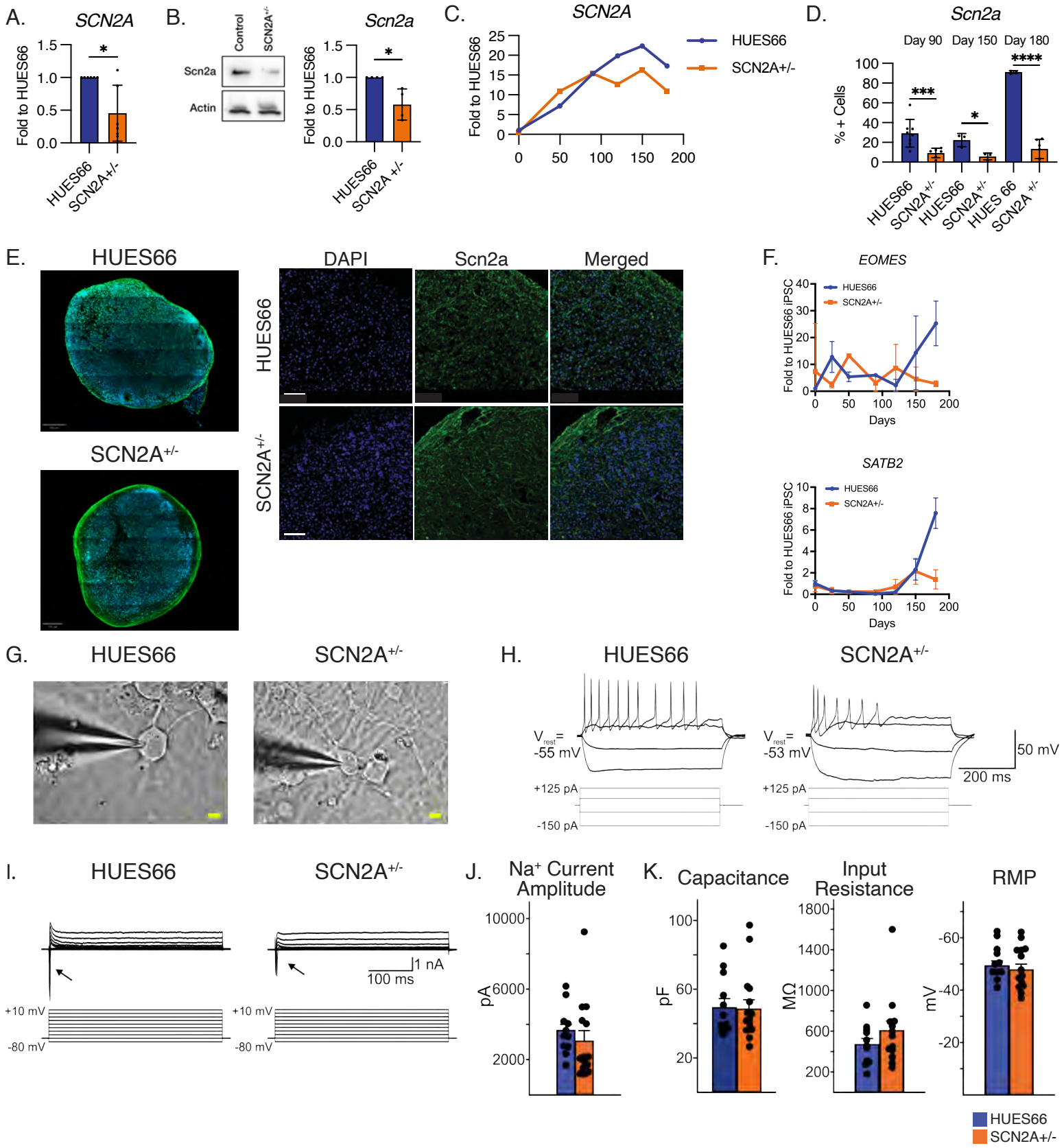
A.
SCN2A
Fold to HUES66
1.5
1.0
0.5
0.0
*
HUES66
SCN2A+/-
B.
Control
SCN2A+/-
Scn2a
Actin
Scn2a
Fold to HUES66
1.5
1.0
0.5
0.0
*
HUES66
SCN2A +/-
C.
SCN2A
Fold to HUES66
25
20
15
10
5
0
0
50
100
150
200
HUES66
SCN2A+/-
D.
Scn2a
Day 90
Day 150
Day 180
% + Cells
100
80
60
40
20
0
***
*
****
HUES66
SCN2A+/-
HUES66
SCN2A+/-
HUES 66
SCN2A+/-
E.
HUES66
SCN2A+/-
DAPI
Scn2a
Merged
HUES66
SCN2A+/-
F.
EOMES
Fold to HUES66 iPSC
40
30
20
10
0
HUES66
SCN2A+/-
0
50
100
150
200
Days
SATB2
Fold to HUES66 iPSC
10
8
6
4
2
0
HUES66
SCN2A+/-
0
50
100
150
200
Days
G.
HUES66
SCN2A+/-
H.
HUES66
SCN2A+/-
Vrest =
-55 mV
+125 pA
-150 pA
Vrest =
-53 mV
+125 pA
-150 pA
50 mV
200 ms
I.
HUES66
SCN2A+/-
1 nA
100 ms
+10 mV
-80 mV
+10 mV
-80 mV
J.
Na+ Current Amplitude
pA
10000
6000
2000
K.
Capacitance
pF
100
60
20
Input Resistance
MΩ
1800
1400
1000
600
200
RMP
mV
-60
-40
-20
HUES66
SCN2A+/-

Figure 2. Characterization of SCN2A mutant stem cells and organoids. (A) RNA expression of SCN2A shows expected 50% reduction in mutant line compared to wildtype. N = 6, SD shown, * $p < 0.05$. (B) Protein expression of Scn2a shows a 50% reduction in mutant line compared to control. N = 6, SD shown, * $p < 0.05$. Full blot images in Supplement. (C) Expression of SCN2A in cortical organoids from day 0 to 180 shows SCN2A expression only decreased in mutant organoids after day 100. N = 6, SEM shown. (D-E) Immunofluorescence of Scn2a in 180-day old organoid sections shows lower levels of Scn2a in mutant organoids, quantified in (D). N= 6, SD shown, * < 0.05. (F) Expression of EOMES and SATB2, as markers for intermediate progenitor cells and upper layer neuron cells, respectively, are decreased in SCN2A-mutant organoids compared to wildtype. (G) Infrared differential interference contrast (IR-DIC) images of Control and $Scn2a^{+/-}$ iNGN2 neurons viewed in the patch-clamp assay recording set up. Scale bar = 10 µm. (H) Sample recorded traces from HUES66 and SCN2A-mutant expressing cells in response to hyperpolarizing and depolarizing current injections. (I) Sample recorded traces of HUES66 and SCN2A-mutant cell current responses following depolarizing voltage steps (10 mV steps from -80 mV to +10 mV). Arrow indicates the presence of transient Na+ currents that are visible starting at ~-40 mV. (J) Summary graphs of Na^+ current amplitudes. (K) Summary graphs of passive cell membrane properties. Plots show mean values ±SEM; N=11 and 14 for HUES66 and $SCN2A^{+/-}$, respectively.

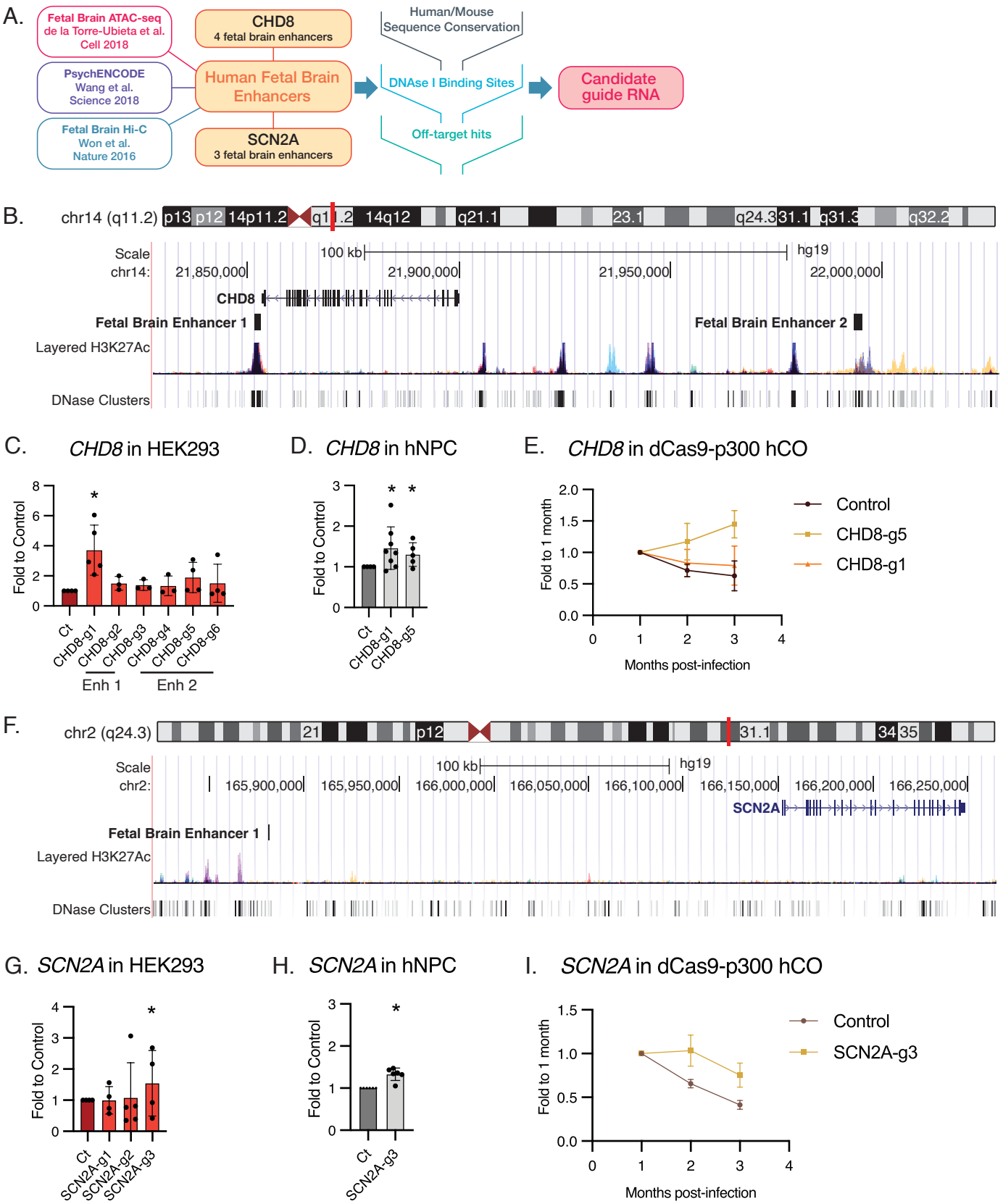
A.
Fetal Brain ATAC-seq
de la Torre-Ubieta et al.
Cell 2018
PsychENCODE
Wang et al.
Science 2018
Fetal Brain Hi-C
Won et al.
Nature 2016
CHD8
4 fetal brain enhancers
Human Fetal Brain Enhancers
SCN2A
3 fetal brain enhancers
Human/Mouse
Sequence Conservation
DNAse I Binding Sites
Off-target hits
Candidate guide RNA
B.
chr14 (q11.2)
Scale
chr14:
100 kb
hg19
21,850,000
21,900,000
21,950,000
22,000,000
CHD8
Fetal Brain Enhancer 1
Fetal Brain Enhancer 2
Layered H3K27Ac
DNase Clusters
C. CHD8 in HEK293
Fold to Control
Ct
CHD8-g1
CHD8-g2
CHD8-g3
CHD8-g4
CHD8-g5
CHD8-g6
Enh 1
Enh 2
D. CHD8 in hNPC
Fold to Control
Ct
CHD8-g1
CHD8-g5
E. CHD8 in dCas9-p300 hCO
Fold to 1 month
Months post-infection
Control
CHD8-g5
CHD8-g1
F.
chr2 (q24.3)
Scale
chr2:
100 kb
hg19
165,900,000
165,950,000
166,000,000
166,050,000
166,100,000
166,150,000
166,200,000
166,250,000
SCN2A
Fetal Brain Enhancer 1
Layered H3K27Ac
DNase Clusters
G. SCN2A in HEK293
Fold to Control
Ct
SCN2A-g1
SCN2A-g2
SCN2A-g3
H. SCN2A in hNPC
Fold to Control
Ct
SCN2A-g3
I. SCN2A in dCas9-p300 hCO
Fold to 1 month
Months post-infection
Control
SCN2A-g3

38 **Figure 3. A stepwise approach to identifying and screening human fetal brain enhancer**
39 **activity.** (A) Workflow for identifying human fetal brain enhancers from previously published
40 datasets and subsequent design and refinement of guide RNA sequences based upon sequence
41 conservation, DNAse I binding, and off-target effects. (B) UCSC Genome browser window
42 highlighting CHD8 in the genome and the two human fetal brain enhancers targeted in this
43 study. (C) Screening *CHD8* guide RNA in HEK293T cells shows an increase in the mRNA
44 expression of a gene of interest for at least one guide per identified enhancer. Expression is
45 measured as fold over empty vector control. N = 4, SD shown, * $p < 0.05$. (D) Successful guide
46 RNA from HEK293T assays were packaged into lentivirus and tested in primary human neural
47 progenitor cells. All tested guide RNA viruses yielded a significant increase in expression of the
48 gene of interest. Expression is measured as fold over empty vector control. N = 5, SD shown, * p
49 < 0.05. (E) RNA expression of CHD8 in dCas9-p300 cortical organoids is significantly increased by
50 guide RNA expression over empty vector control up to 3 months post-infection. Measurement
51 of gene expression is relative to sample collected at 1-month post-infection. N = 3, SD shown.
52 (F) UCSC Genome browser window highlighting SCN2A in the genome and the human fetal brain
53 enhancer targeted in this study. (G) Screening *SCN2A* guide RNA in HEK293T cells shows an
54 increase in the mRNA expression of a gene of interest. Expression is measured as fold over
55 empty vector control. N = 4, SD shown, * $p < 0.05$. (H) SCN2A guideRNA significantly increased
56 gene expression in human neural progenitor cells. N = 6, SD shown, * $p < 0.05$. (I) RNA
57 expression of SCN2A in dCas9-p300 cortical organoids is significantly increased by guide RNA
58 expression over empty vector control up to 3 months post-infection. Measurement of gene
59 expression is relative to sample collected at 1-month post-infection. N = 3, SD shown.

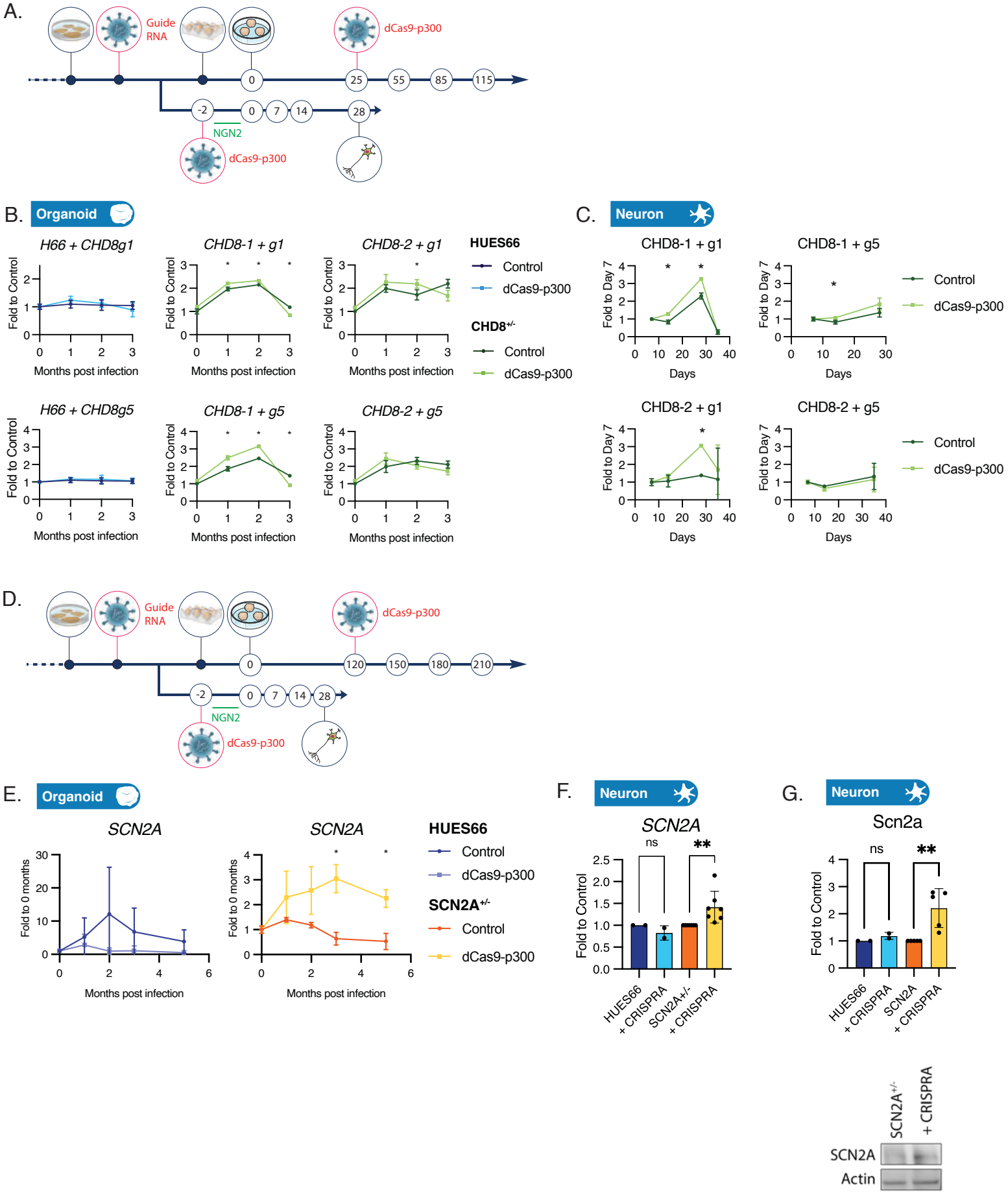
A.
Guide RNA
dCas9-p300
0
25
55
85
115
-2
0
7
14
28
NGN2
dCas9-p300
B.
Organoid
H66 + CHD8g1
CHD8-1 + g1
CHD8-2 + g1
H66 + CHD8g5
CHD8-1 + g5
CHD8-2 + g5
Fold to Control
Months post infection
HUES66
Control
dCas9-p300
CHD8+/-
Control
dCas9-p300
C.
Neuron
CHD8-1 + g1
CHD8-1 + g5
CHD8-2 + g1
CHD8-2 + g5
Fold to Day 7
Days
Control
dCas9-p300
D.
Guide RNA
dCas9-p300
0
120
150
180
210
-2
0
7
14
28
NGN2
dCas9-p300
E.
Organoid
SCN2A
SCN2A
Fold to 0 months
Months post infection
HUES66
Control
dCas9-p300
SCN2A+/-
Control
dCas9-p300
F.
Neuron
SCN2A
ns
**
Fold to Control
HUES66
+ CRISPRA
SCN2A+/-
+ CRISPRA
G.
Neuron
Scn2a
ns
**
Fold to Control
HUES66
+ CRISPRA
SCN2A
+ CRISPRA
SCN2A+/-
+ CRISPRA
SCN2A
Actin

Figure 4. CRISPR-A treatment of mutant organoids and neurons leads to increased expression of CHD8 and SCN2A. (A) Workflow for infection of CHD8-mutant organoids or iNGN2 neurons. Guide RNA are first transduced into cell lines and sorted by GFP. dCas9-p300 is transduced into the cells during differentiation; for iNGN2 neurons, at day -2 of the protocol and day 25 for cortical organoids. (B) CHD8 expression in organoids treated with CRISPR-A shows modest increases in CHD8 expression, lost after 3 months post-infection. No increase in expression is observed in HUES66 organoids. (C) CHD8 mRNA expression is increased in CHD8-mutant iNGN2 neurons transduced with CRISPR-A. Neurons were collected at day 7, 14, 28, and 35 post-initiation. (D) Workflow for infection of SCN2A-mutant organoids or iNGN2 neurons. Guide RNA are first transduced into cell lines and sorted by GFP. dCas9-p300 is transduced into the cells during differentiation; for iNGN2 neurons, at day -2 of the protocol and day 120 for cortical organoids. (E) SCN2A expression is rescued in mutant organoids but not wildtype. Organoids were infected at day 120 and collected 1-5 months post-infection. Expression shown as fold to 1-month post-infection control. (F) Expression of SCN2A is rescued by CRISPR-A in SCN2A-mutant neurons but not wildtype. Expression in wildtype (HUES66) is unchanged by CRISPR-A, whereas expression is significantly increased in the mutant line. N = 7, SD shown, * $p < 0.05$. (G) Expression of Scn2a protein is significantly increased by CRISPR-A in mutant line but not in wildtype. N = 5, SD shown, * $p < 0.05$.

Neuron

A.

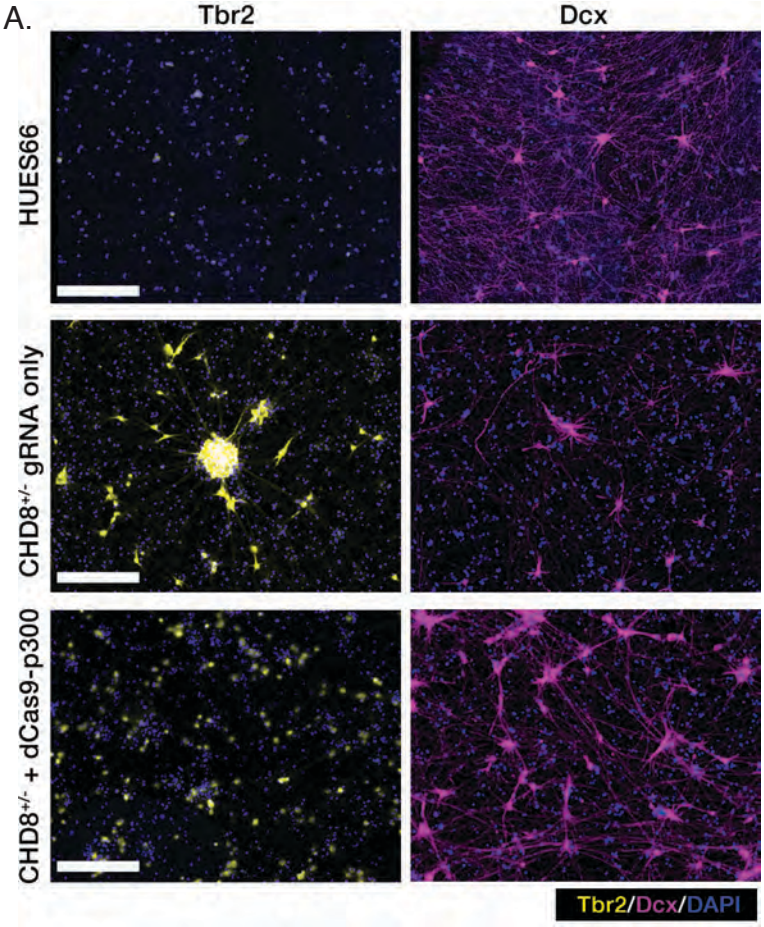

B.

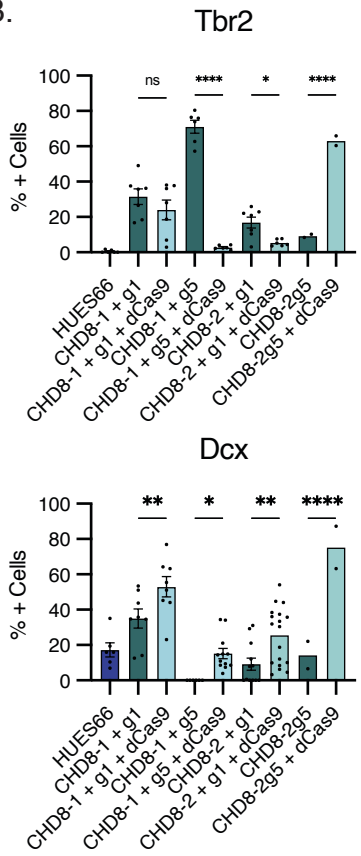

C.

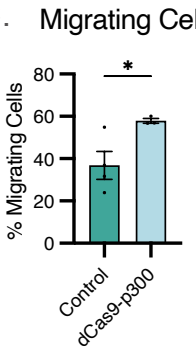

D.

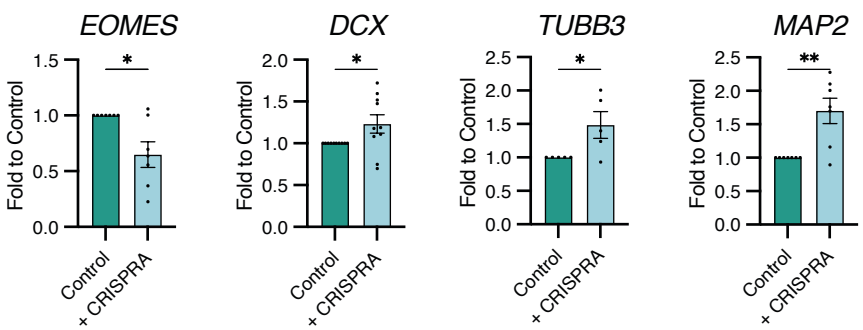

Organoid

E.

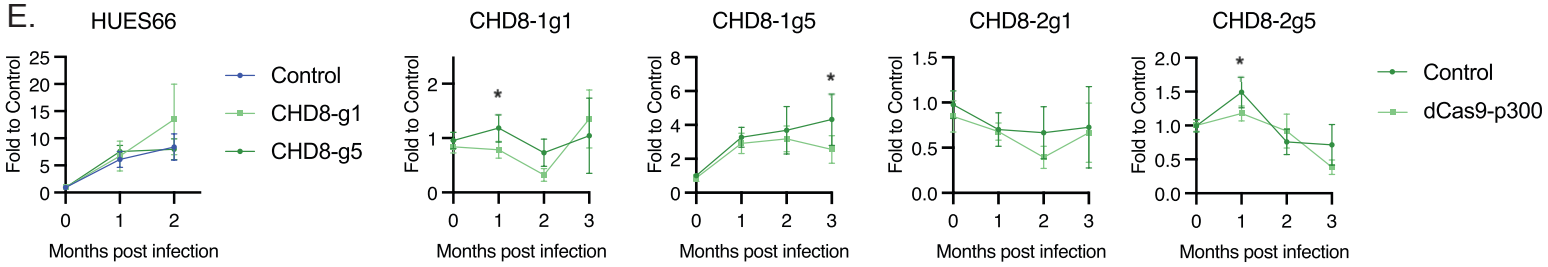

F.

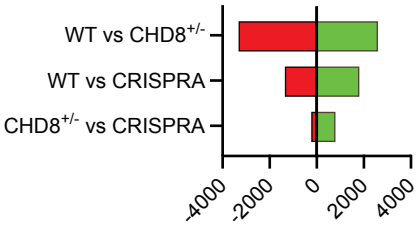

G.

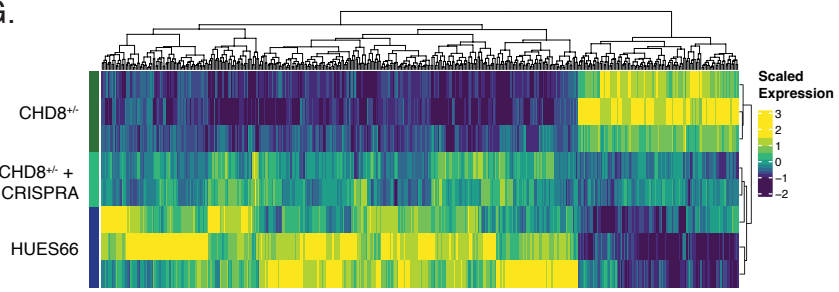

H.

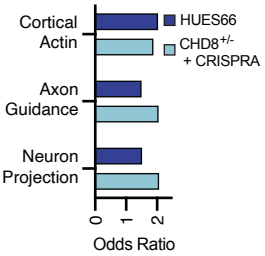

Figure 5. Aberrant phenotypes are reversed with CHD8 CRISPR-A treatment. (A) Expression of Tbr2 and Dcx in CHD8-mutant iNGN2 neurons with and without dCas9-p300. (B) Quantification of immunofluorescence images show Tbr2 expression is significantly decreased by CRISPR-A treatment while Dcx is significantly increased, suggesting increased maturity of the neurons. (C) Increase in Dcx+ cells on cell processes shows a significant increase in migrating neurons in CRISPR-A treated iNGN2 cultures. N = 5, SD shown, * $p < 0.05$. (D) Expression of cell type markers EOMES (Tbr2), DCX, TUBB3, and MAP2 in iNGN2 neurons shows an increase in neuron maturity with CRISPR-A treatment. N = 5, SD shown, * $p < 0.05$. (E) Organoid size is significantly reduced by CRISPR-A treatment. Measurements taken at day 25 when organoids were initially infected and every month post infection for 3 months. N = 50, SEM shown, * $p < 0.05$. (F) Significant (padj < 0.05) differentially expressed genes (DEGs) from bulk RNAseq in hCO 1-month post-infection with CRISPR-A. Compared to $CHD8^{+/-}$ hCO, HUES66 hCO show a high number of both upregulated and downregulated DEGs. Treatment of $CHD8^{+/-}$ with CRISPR-A decreased the number of DEGs compared to HUES66. $CHD8^{+/-}$ hCO treated with CRISPR-A show a larger proportion of upregulated than downregulated DEGs. (G) Heatmap of DEG expression shows CRISPR-A treatment induces a change in gene expression pattern towards wildtype organoids (HUES66). (H) Shared Gene Ontology terms related to neuron development are significantly upregulated in both wildtype and CRISPR-A treated mutant hCO relative to control-treated hCO.

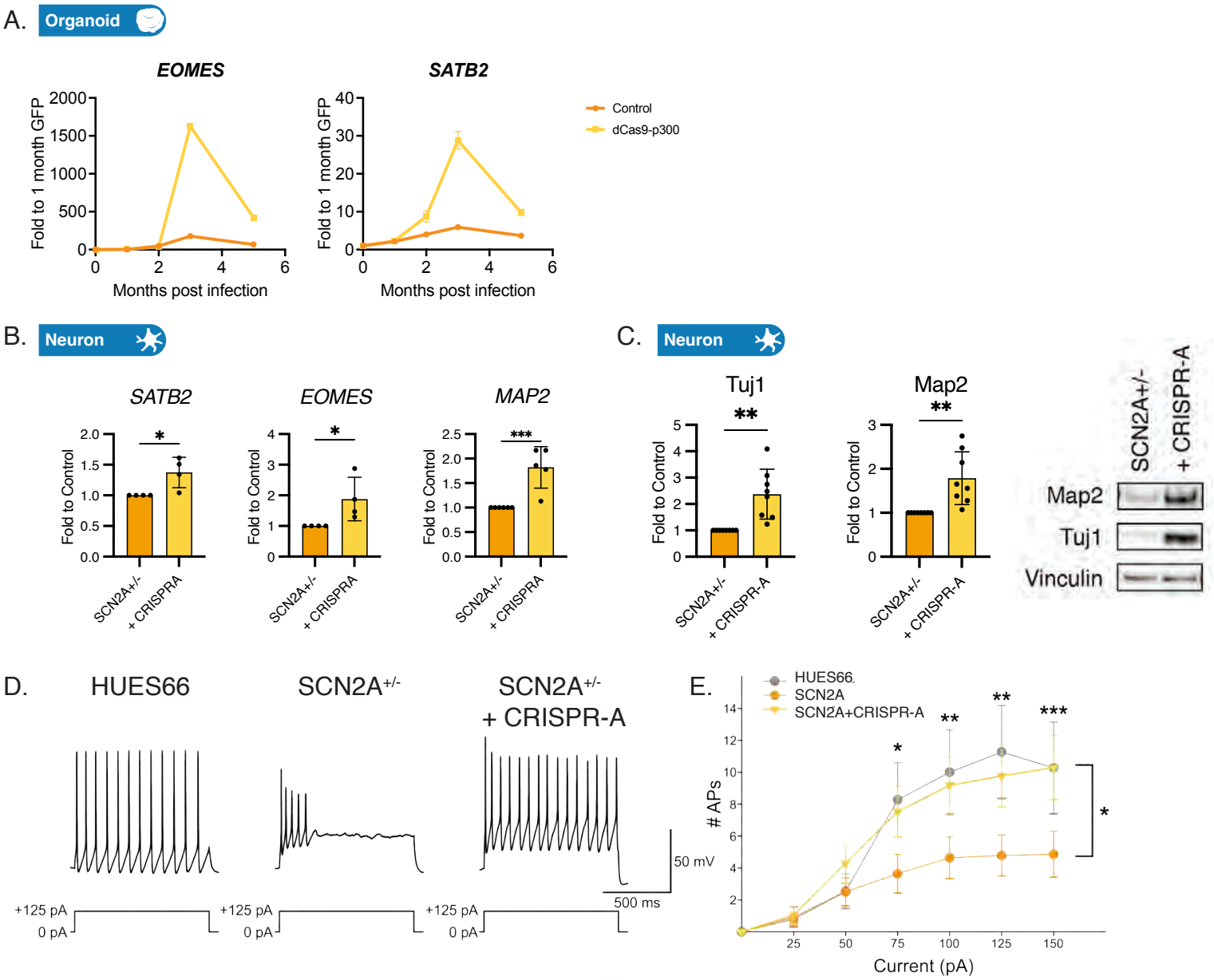
A.
Organoid
EOMES
SATB2
Fold to 1 month GFP
Months post infection
Control
dCas9-p300
B.
Neuron
SATB2
EOMES
MAP2
Fold to Control
SCN2A+/-
+ CRISPRA
C.
Neuron
Tuj1
Map2
Fold to Control
SCN2A+/-
+ CRISPR-A
Map2
Tuj1
Vinculin
D.
HUES66
SCN2A+/-
SCN2A+/-
+ CRISPR-A
+125 pA
0 pA
50 mV
500 ms
E.
HUES66
SCN2A
SCN2A+CRISPR-A
APs
Current (pA)

Figure 6. Aberrant phenotypes are reversed with SCN2A CRISPR 96-A treatment. (A) Expression of *EOMES* and *SATB2*, as markers for intermediate progenitor cells and upper layer neuron cells, respectively, are increased with CRISPR-A treatment of SCN2A-mutant organoids. N = 3-8, SEM shown. (B) Expression of *EOMES* and *SATB2* are increased with CRISPR-A treatment of SCN2A-mutant neurons. N = 5, SD shown, * $p < 0.05$. (C) Expression of Tuj1 and Map2 are significantly increased by CRISPR-A treatment of SCN2A-mutant neurons. N = 8, SD shown, * $p < 0.05$. Full blot images in Supplement. (D) Sample excitability traces from Control, $SCN2A^{+/-}$, and $SCN2A^{+/-}$ +CRISPR-A cells show partial rescue of sustained neuronal firing activity in response to a depolarizing current pulse (+125 pA, 1 sec). Cells were held at a membrane potential of -60 mV prior to current injection. (E) Graph comparing the number of action potentials (APs) fired in response to increasing current injections (1 sec). CRISPR-A treatment of mutant neurons significantly rescued the number of action potentials fired per injected current (N=11, N=14 and N=17 for HUES66, $SCN2A^{+/-}$, and $SCN2A^{+/-}$ +CRISPR-A, respectively). Plots depict mean number of action potentials ±SEM. Two-way repeated ANOVA revealed a significant difference between $SCN2A^{+/-}$ and $SCN2A^{+/-}$ +CRISPR-A distributions, indicated by * $p < 0.05$. Bonferroni *posthoc* analysis further showed significant differences at each level of current injection, where * $p < 0.05$, ** $p < 0.01$ and *** $p < 0.001$.